Title

Molecular design of an ultra-strong tissue adhesive hydrogel with tunable multifunctionality.

Authors

Zheng, Yuting
Baidya, Avijit
Annabi, Nasim

Publication Date

2023-11-01

DOI

10.1016/j.bioactmat.2023.06.007

Peer reviewed

Bioactive Materials 29 (2023) 214–229

Contents lists available at ScienceDirect

Bioactive Materials

journal homepage: www.keaipublishing.com/en/journals/bioactive-materials

Molecular design of an ultra-strong tissue adhesive hydrogel with tunable multifunctionality

Yuting Zheng [a], Avijit Baidya [a], Nasim Annabi [a,b,*]

[a] Department of Chemical and Biomolecular Engineering, University of California, Los Angeles, Los Angeles, CA, 90095, United States
[b] Department of Bioengineering, University of California, Los Angeles, Los Angeles, CA, 90095, United States

ARTICLE INFO

Keywords:
Molecular engineering
Tough hydrogel
Bioadhesive
Multifunctionality

ABSTRACT

Designing adhesive hydrogels with optimal properties for the treatment of injured tissues is challenging due to the tradeoff between material stiffness and toughness while maintaining adherence to wet tissue surfaces. In most cases, bioadhesives with improved mechanical strength often lack an appropriate elastic compliance, hindering their application for sealing soft, elastic, and dynamic tissues. Here, we present a novel strategy for engineering tissue adhesives in which molecular building blocks are manipulated to allow for precise control and optimization of the various aforementioned properties without any tradeoffs. To introduce tunable mechanical properties and robust tissue adhesion, the hydrogel network presents different modes of covalent and noncovalent interactions using *N*-hydroxysuccinimide ester (NHS) conjugated alginate (Alg-NHS), poly (ethylene glycol) diacrylate (PEGDA), tannic acid (TA), and Fe^{3+} ions. Through combining and tuning different molecular interactions and a variety of crosslinking mechanisms, we were able to design an extremely elastic (924%) and tough (4697 kJ/m^3) multifunctional hydrogel that could quickly adhere to wet tissue surfaces within 5 s of gentle pressing and deform to support physiological tissue function over time under wet conditions. While Alg-NHS provides covalent bonding with the tissue surfaces, the catechol moieties of TA molecules synergistically adopt a mussel-inspired adhesive mechanism to establish robust adherence to the wet tissue. The strong adhesion of the engineered bioadhesive patch is showcased by its application to rabbit conjunctiva and porcine cornea. Meanwhile, the engineered bioadhesive demonstrated painless detachable characteristics and *in vitro* biocompatibility. Additionally, due to the molecular interactions between TA and Fe^{3+}, antioxidant and antibacterial properties required to support the wound healing pathways were also highlighted. Overall, by tuning various molecular interactions, we were able to develop a single-hydrogel platform with an "all-in-one" multifunctionality that can address current challenges of engineering hydrogel-based bioadhesives for tissue repair and sealing.

1. Introduction

Hydrogels, water-swollen polymeric crosslinked networks, are capable of interacting with the tissues through physical or chemical interactions and are extensively employed in the design of bioadhesive biomaterials [1,2]. However, most bioadhesives either suffer from cohesive failure due to a lack of mechanical strength or adhesive failure resulting from insufficient tissue-biomaterial interfacial interactions [3–7]. Furthermore, incorporation of additional functionalities in these adhesive hydrogels such as antibacterial and antioxidant properties that are critical for wound healing can be challenging. Mechanistically, molecular interactions enable crosslinking among polymeric backbones, forming the primary skeleton of hydrogel constructs. These crosslinked molecular domains eventually modulate the hydrogel's mechanical properties, including toughness, stretchability, stiffness, and others. Meanwhile, the functional groups present in these crosslinked networks introduce other important features such as adhesive, antibacterial, and antioxidant properties [8]. Therefore, the ability to tune the crosslinking density while maintaining desired physicochemical properties is imperative in designing bioadhesive hydrogels.

Engineering bioadhesive hydrogels with optimal cohesive properties that mimic the stiffness and elasticity of native tissues is challenging

Peer review under responsibility of KeAi Communications Co., Ltd.
* Corresponding author. Department of Chemical and Biomolecular Engineering, University of California, Los Angeles, Los Angeles, CA, 90095, United States.
E-mail address: nannabi@ucla.edu (N. Annabi).

https://doi.org/10.1016/j.bioactmat.2023.06.007
Received 1 November 2022; Received in revised form 15 May 2023; Accepted 8 June 2023

since most engineered hydrogel-based bioadhesives are fragile and weak [1,7,9–12]. In addition, there is often a tradeoff among different mechanical properties of hydrogels, compromising their applicability as a potential structural biomaterial for medical use. For example, increasing the ultimate strength often reduces the stretchability, and improving the toughness may drop the stiffness of the hydrogel-based biomaterials [13–18]. Furthermore, most bioadhesive hydrogels reported thus far have been prone to fracture and breakage when subjected to sub-MPa tensile stress or high-extent deformation. They have also displayed breaking energies around one percent of biological tissues such as cartilage [19]. To address these limitations, different strategies have been implemented to modify the crosslinking mechanism of hydrogel networks, including the formation of double network (DN) hydrogels [20], nanocomposite hydrogels [5], sliding-ring hydrogels [21], resilin-based hydrogels [22], topological hydrogels [23], macromolecular crosslinked networks [24], and interpenetrating network hydrogels [25]. However, achieving a high tensile strength and Young's modulus without compromising elasticity to better reflect the nature of soft elastic tissue (i.e., lung and heart) remains an unsolved issue. For instance, Daniela et al. [26] prepared photocrosslinkable gellan gum (MeGG) hydrogels combined with an ionic crosslinking system with an ultimate strength of ~800 kPa, but due to the tradeoff between ionic crosslinking and the degree of methacrylation, no improvement was achieved in Young's modulus (<20 kPa) and strain (<80%). While the stiffness could be improved by increasing the degree of methacrylation, the strain and ultimate strength were shown to significantly decrease. Recently, a hydrogen-bond-mediated, pseudo-slide-ring networked hydrogel, synthesized with carboxymethylated polyrotaxanes and polyacrylamides (PAAm), showed an enhanced Young's modulus and ultimate strength upon increasing the number of hydrogen-bonding pairs. However, the stretchability did not increase in parallel with the Young's modulus and strength, as their - process generated a rigid hydrogen-bonded network that in turn diminished the mobility of the carboxymethylated α-cyclodextrins within the crosslinked hydrogel [27]. In addition, not only the use of acrylamide moieties potentially reduced the biocompatibility [28], but also the multi-step synthesis procedure increasedthe complexity of the system, hindering the clinical translation of this hydrogel. Meanwhile, as native soft tissues exist across a wide range of mechanical properties with the Young's modulus ranging from 3 kPa for the kidney to 100 kPa for the skin [29], it is essential to achieve control over the bioadhesive's crosslinking mechanisms and the resulting mechanical properties in order to achieve tissue-mimicking mechano-physical properties, and eliminate inflammation induced by mechanical mismatch [30]. Another challenge includes maintaining the mechanical integrity of the bioadhesives under wet physiological conditions over time. The stiffness of bioadhesive hydrogels can drop due to either their unstable crosslinking resulting in hydrogels' network dissociation or degradation [31,32] or the excessive swelling of the hydrophilic networks [33–37]. Therefore, there is an unmet need for a biocompatible hydrogel platform featuring a programmable crosslinking mechanism which allows for fine tuning of a single material property (e.g., stiffness, toughness, stretchability, ultimate strength) without compromising others. In addition to the improved cohesion achieved by modulating the crosslinking mechanism, the wet tissue adhesive properties of these biomaterials are also important for their applications as sealants or glues for sealing injured internal organs.

Specially for the closure of internal wounds, adhesive hydrogels are an alternative to sutures and staples [38–40]. The retention of these bioadhesives on injured tissue surfaces throughout the healing process while supporting physiological tissue function is critical. Two main design strategies have been used to impart wet tissue adhesion to hydrogels: **1)** *in situ* formation of adhesive hydrogels on wet tissues from precursor solutions, and **2)** adhesion of prefabricated patches to the wet tissue surfaces [1,38,41,42]. However, both design strategies face limitations. For example, many *in situ*-forming adhesive hydrogels require the use of an external device, such as a light source [4,43–45] or co-injector delivery system [46,47], while others require adding/-spraying crosslinkers [48,49] or mixing different components [50], not only further complicating the design but also making the gelation inhomogeneous. These extra steps can be fatal in urgent, life-threatening situations. In addition, traditional bioadhesives only demonstrate strong adhesion to dry substrates in air and cannot effectively seal wet organs [11,51]. Slow gelation presents another limitation for the clinical application of these hydrogels. For example, Juan et al. successfully prepared a bioadhesive prepolymer solution for *in situ* gelation based on tannic acid (TA) and silk fibroin, but the gelation process did not occur until after 9.5 h [52]. In another study, Younseon et al. made a phenol-amine superglue with an adhesive strength of 3.87 MPa, but the required curing time was 12 h [53]. A slow gelation time can render the bioadhesive ineffective as it cannot prevent excessive blood loss and seal leakages or apply to dynamic organs such as the heart or lungs. In addition, body fluids may foul or dilute the prepolymer solution before effective gelation *in situ*. On the other hand, a rapid gelation process also presents complications with handling of the bioadhesive material by clinicians. In many existing studies on prefabricated adhesive patches, there is an unspecified or a prolonged incubation or contact time (>2 h) necessary for the patch to achieve robust adhesion [1,38,42,54–57]. Additionally, previously reported hydrogel-based adhesives demonstrate insufficient sealing strength (with most having an adhesive strength of less than 40 kPa to the skin tissue) and short-term adhesion [7,58,59]. Furthermore, current bioadhesives have shown limited characteristics in different surgical applications. For example, Xin et al. prepared an ultra-fast self-gelling powder that could crosslink *in situ* within 2 s; however, the hydrogel crosslinking was highly pH-dependent, limiting its usage for internal organs with acidic environments such as the stomach [60]. Moreover, it remains an obstacle to achieve both a strong cohesion and adhesion simultaneously [3–7,61], while also allowing for painless detachment in situations involving misplacement, the need to adjust the material, or implanted device retrieval. To the best of our knowledge, few bioadhesives developed so far have demonstrated robust and rapid adhesion along with trigger-induced detachability [62]. Therefore, there is an unmet clinical need for bioadhesives which are designed *via* their molecular domains to incorporate multi-mode crosslinking sites that appropriately modulate network mechanics and functionalities while also facilitating tissue-material interfacial interactions.

Incorporating multiple functionalities (e.g., antimicrobial properties) into bioadhesive hydrogels is an important step to make them suitable for both sealing and repairing internal wounds. For example, researchers have incorporated different antimicrobial peptides [11], antibacterial nanomaterials such as silver nanoparticles [63], and antibiotics [64] into bioadhesives to provide them with antibacterial properties. In addition, different chemical functional groups such as quaternary ammoniums [65] have been conjugated to bioadhesives to make them antimicrobial. However, these methods require additional steps during synthesis that often involved expensive and sensitive materials, which may cause issues such as cytotoxicity or bacterial resistance, and provide only short-term antibacterial effects due to leaching of antibiotics or nanomaterials out of the polymeric network [66].

To address the need for designing multifunctional adhesive biomaterials with antimicrobial properties for the treatment of different injured tissues, we aimed to develop an elastic and tough hydrogel patch that adheres to wet tissues after a few seconds of pressing while supporting the tissues' physiological functions. This multifunctional patch, entitled APTF hydrogel, was composed of a poly (ethylene glycol) diacrylate (PEGDA) hydrogel interpenetrated with *N*-hydroxysuccinimide ester (NHS)-conjugated alginate (Alg-NHS) and subsequently treated with TA/Fe^{3+} to achieve robust cohesion and adhesion. We showed tunability of the mechanical and adhesive properties of the hydrogel by controlling a series of covalent and non-covalent interactions among Alg-NHS, PEGDA, TA and Fe^{3+} that collectively formed a multi-

component macromolecular system. While the covalent network of PEGDA defined the primary backbone of the hydrogel, the reversible hydrogen bonding between PEGDA and TA and ionic interactions between Alg-NHS and Fe^{3+} together provided excellent elasticity and toughness. As such, stiffness, ultimate strength, and toughness could be improved significantly without compromising stretchability. The robust adhesive nature of the hydrogel was achieved by chemically conjugating NHS to alginate strands and incorporating the mussel-inspired adhesive moieties presented by TA; the synergy effect of these two adhesive moieties enhanced the adhesion strength of the resulting hydrogel. Strong adherence of the designed bioadhesive was demonstrated on rabbit conjunctiva and porcine cornea. Further, painless detachment of the patch was also easily achieved upon the addition of nontoxic chemical agents to the tissue-material interface. Meanwhile, the engineered hydrogel showed excellent antioxidant and antibacterial properties due to the presence of the TA/Fe^{3+} complexes that are essential for wound treatment. The biocompatibility of this multifunctional bioadhesive was assessed *in vitro* using 3T3 cells. Overall, through molecular engineering, the designed hydrogels demonstrated selectively tunable mechanical and physiochemical properties to not only facilitate the closure and treatment of internal and external injuries, but also to potentially promote wound healing.

2. Results and discussion

2.1. Synthesis of APTF adhesive hydrogel based on alginate (Alg)-NHS, PEGDA, and TA/Fe^{3+}

Sequential synthesis of the APTF adhesive hydrogel patch comprised of Alginate (Alg)-NHS, PEGDA and TA/Fe^{3+} is demonstrated in Scheme 1a. First, Alg-NHS and PEGDA were separately synthesized as the primary molecular backbone of the resulting APTF hydrogel. NHS was conjugated to Alg to provide instant tissue-material interfacial interactions and to fine-tune the ionic interactions with Fe^{3+} to control the mechanical properties. TA was also introduced to enrich the crosslinking network by forming dynamic H-bonding interactions with PEGDA, and ion-induced chelation with Fe^{3+} to further tune the mechanical properties while providing multiple functions (i.e., antioxidant and antibacterial properties) for the hydrogel. Additionally, the mussel-inspired adhesive characteristics of TA, along with NHS functionalization onto Alg, provided enhanced tissue adhesion to the resulting APTF hydrogel. The covalent and noncovalent interactions among various macromolecules in the designed hydrogel were used to tune its physical properties. Specifically, the mixture of Alg-NHS/PEGDA prepolymer solution was treated under visible blue light (405 nm) in the presence of lithium phenyl-2,4,6-trimethylbenzoylphosphinate (LAP) photoinitiator to form a covalently interconnected PEGDA network interpenetrated with Alg-NHS, making the primary hydrogel network (AP hydrogel). A secondary molecular network was then established with the addition of TA molecules, which facilitated the formation of H-bonding between oxygen-rich PEGDA backbones. Meanwhile, an ionic crosslinking network was formed inside the hydrogel through the incorporation of Fe^{3+} ions, which could interact with both TA and Alg-NHS, leading to the resulting APTF hydrogel patch, an "all-in-one" crosslinked network.

The molecular interactions inside the synthesized hydrogel, comprised of multiple macromolecular moieties, are demonstrated in Scheme 1b. Initially, PEGDA molecules formed hydrogen bonds with multiple OH groups presented in TA (Scheme1b–i). In a previous study, although PEGDA/TA hydrogels were shown to provide improved toughness and wet tissue adhesion in comparison to PEGDA hydrogels, th reported ultimate strengths were below 80 kPa, and the materials demonstrated limited tunability in mechanical properties [6]. Additionally, the PEGDA/TA hydrogels lacked multifunctionalities [6]. Metal–phenolic networks have recently attracted interest because of

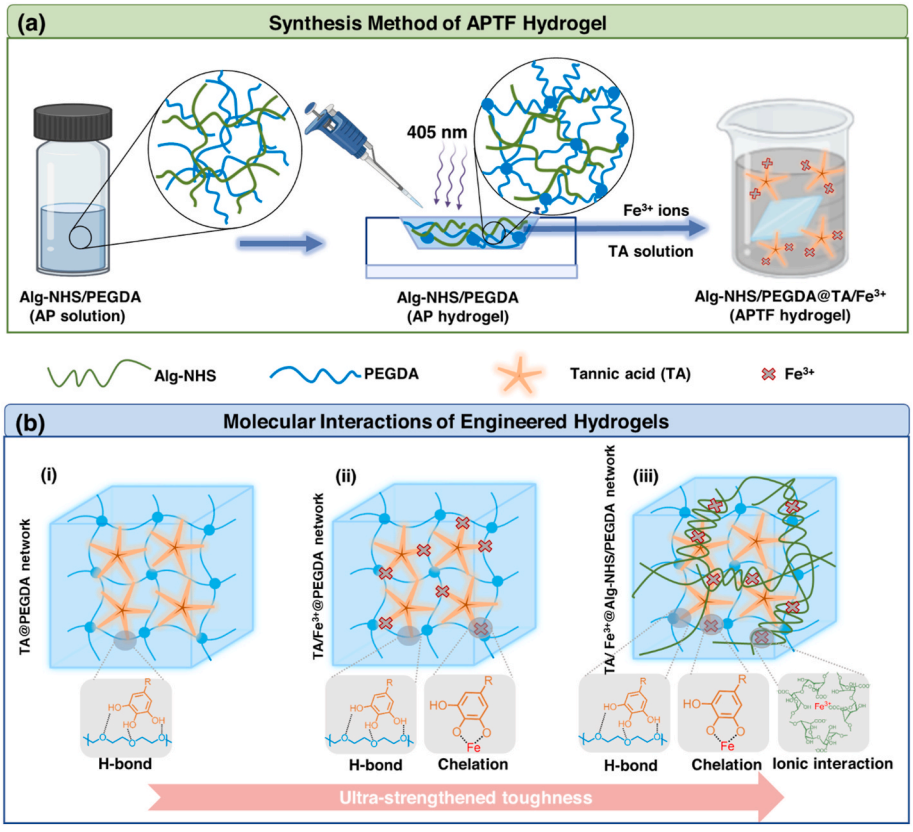

Scheme 1. **(a)** Schematically illustrated synthesis of APTF hydrogel based on Alg-NHS, PEGDA, and TA/Fe^{3+}. **(b)** Molecular interactions among the building blocks of APTF hydrogel: **(i)** TA crosslinked PEGDA network **(ii)** TA/Fe^{3+} crosslinked PEGDA network and **(iii)** TA/Fe^{3+} crosslinked AP network.

their desirable properties [67,68]. In particular, Fe^{3+}-phenolic chelation is of particular interest for its broad functionalities, including hemostatic, antioxidant and photothermal properties [7,69,70]. Therefore, it would be highly desirable to incorporate Fe^{3+} into PEGDA/TA adhesive hydrogels to further enhance their properties. However, the facile mono-chelation between TA and Fe^{3+} may interfere with the H-bond interactions between PEGDA and TA, leading to a drop in mechanical properties (Scheme1b-ii). To eliminate this tradeoff, we incorporated Alg-NHS, which competes with TA for Fe^{3+} ions, in the hydrogel network to increase the dynamic crosslinking densities *via* ionic crosslinking with Fe^{3+} ions, while also re-introducing the H-bond interactions between TA and PEGDA. Furthermore, synergistic adhesion was achieved through utilizing both TA and NHS to form a wide range of both covalent and noncovalent interactions with the tissues. By controlling the multi-mode molecular interactions, the crosslinking mechanisms in the resulting APTF hydrogel network were modulated, leading to the formation of an ultra-strengthened multi-component adhesive patch (Scheme1b-iii).

2.2. Synthesis and chemical characterizations of Alg-NHS, AP, and APTF hydrogel

A schematic for the synthesis of NHS-modified Alg based on the EDC/NHS coupling reaction is presented in Fig. 1a. The resulting Alg-NHS was chemically characterized with proton nuclear magnetic resonance (^{1}H NMR), showing the presence of succinimide hydrogen peak at 2.8 ppm (Fig. 1b). To increase the NHS content in the Alg backbone, the Alg: EDC:NHS ratio was varied from 1:1:1 to 1:2:10 to 1:4:20. An increase in

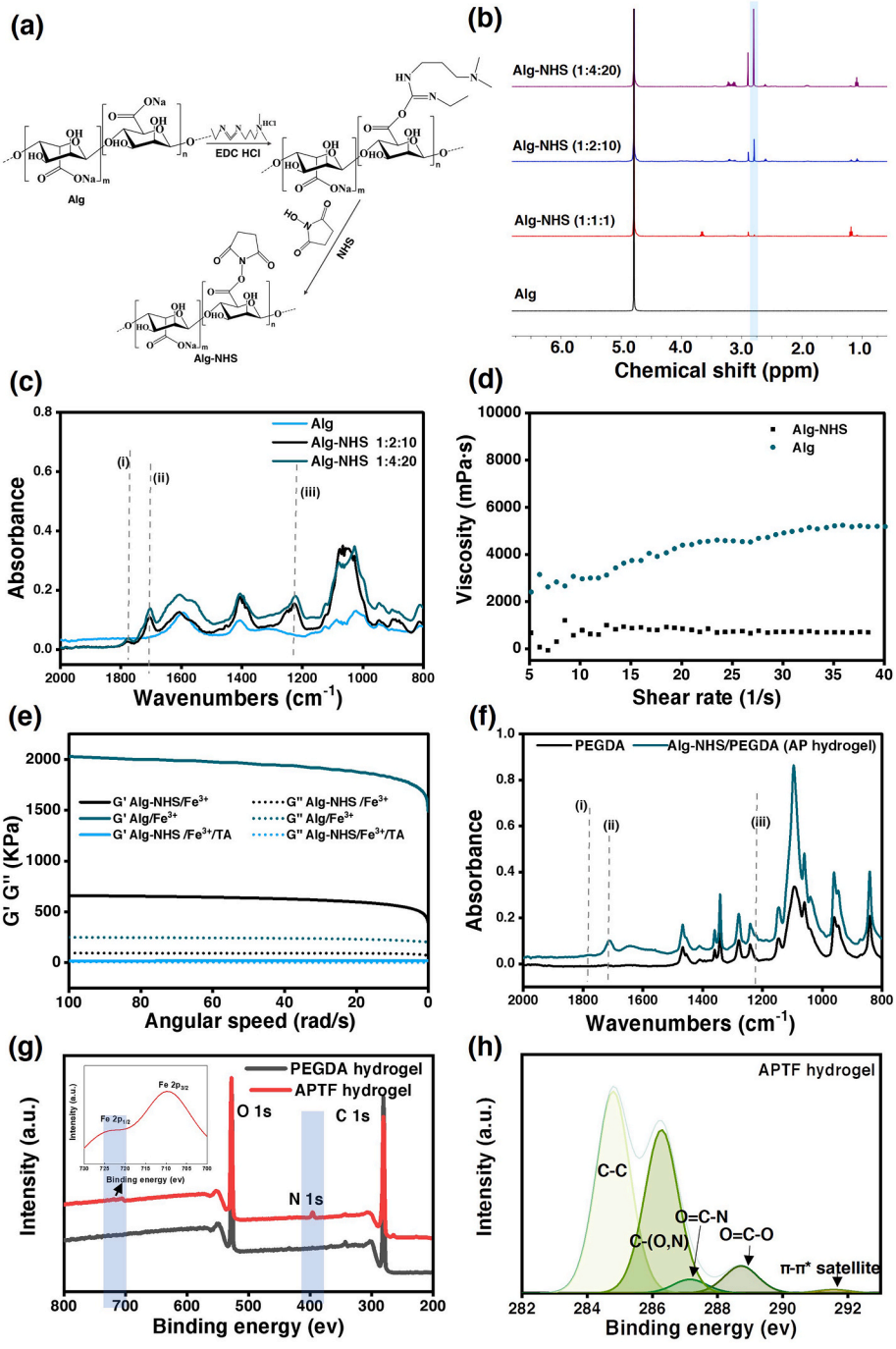

Fig. 1. Characterizations of synthesized Alg-NHS, AP hydrogel, APTF hydrogel. **(a)** Schematic for Alg-NHS synthesis. **(b)** ^{1}H NMR and **(c)** FTIR spectra of Alg, Alg conjugated with NHS under different reaction conditions. FTIR spectra showing **(i)** carbonyl stretch of NHS (1780 cm^{-1}), **(ii)** carbonyl stretch of NHS (1704 cm^{-1}), **(iii)** CNC stretch of NHS (1219 cm^{-1}). **(d)** The viscosity of synthesized Alg-NHS and Alg at 2%. **(e)** Rheology characterizations (G′, G″) of Alg/Fe^{3+}, Alg-NHS/Fe^{3+}, and Alg-NHS/TA/Fe^{3+} hydrogel, the concentrations of Alg, Fe^{3+} and TA in this study were 2%, 3% and 40% respectively. **(f)** FTIR spectra of photocrosslinked PEGDA hydrogel (22%) and AP hydrogel consisting of 8% Alg-NHS and 22% PEGDA: **(i)** carbonyl stretch of NHS (1780 cm^{-1}), **(ii)** carbonyl stretch of NHS (1704 cm^{-1}), **(iii)** CNC stretch of NHS (1219 cm^{-1}). **(g)** XPS survey of PEDGA and APTF hydrogel. **(h)** Carbon XPS of APTF hydrogel.

the degree of NHS conjugation in Alg-NHS was confirmed by the enhanced NHS peak intensity in the ^{1}H NMR spectrum of Alg-NHS formed by using higher Alg:EDC:NHS ratio (Fig. 1b). Successful conjugation of NHS onto Alg was further analyzed with FTIR spectroscopy, which showed characteristic NHS peaks at 1780 cm^{-1} (carbonyl stretch of NHS), 1704 cm^{-1} (carbonyl stretch of NHS), 1219 cm^{-1} (C–N–C stretch of NHS) (Fig. 1c).

The viscosity of the Alg-NHS solution was measured and compared to that of a native Alg solution, as shown in Fig. 1d, revealing a lower viscosity for Alg-NHS. Since NHS groups are covalently attached to the carboxyl groups of the Alg moieties which contain two hydrogen bonding, they can restrict the electrostatic interactions of Alg by reducing the negative charge of the carboxyl group. This replaces the electrostatic interactions with dynamic and comparatively weaker hydrogen bonding interactions, reflected in the lowered viscosity of Alg-NHS (2%) compared with that of native Alg (2%) [71].

Both Alg-NHS and TA can interact with Fe^{3+} ions. To understand the effect of Alg-NHS and TA in their cross-interactions with Fe^{3+}, rheological studies were performed on Alg-NHS/Fe^{3+} hydrogels and Alg-NHS/TA/Fe^{3+} hydrogels (ATF hydrogels), and the results were compared with those of the Alg/Fe^{3+} hydrogel (Fig. 1e). While native Alg with bare COOH groups formed a stronger hydrogel with Fe^{3+} ions, the presence of NHS could tune the mechanical properties of the resulting hydrogel by reducing the "egg-box" crosslinking density. Meanwhile, when Fe^{3+} was chelated with TA, it still interacted with Alg-NHS to form a weak hydrogel. This was confirmed upon observing a greater elastic modulus (G′) than the viscous modulus (G″). However, the G′ and G″ were lower in the hydrogels containing TA as compared to those without TA. Therefore, we hypothesized that both TA and Alg-NHS may compete for interacting with Fe^{3+}. Overall, by introducing NHS and TA into the Alg/Fe^{3+} network, the molecular interactions and crosslinking densities across the APTF hydrogels were manipulated to tune their mechanical properties.

As a key functional moiety for tuning tissue-material interfacial interactions [1,72,73], NHS presence within the AP hydrogel was assessed *via* FTIR measurements shown in Fig. 1f. Peaks at 1780 cm^{-1} and 1704 cm^{-1} in the FTIR spectra of the AP hydrogel are related to the carbonyl stretching of NHS. The peak at 1219 cm^{-1} corresponds to C–N–C stretch of NHS. Formation of APTF hydrogel was also assessed with X-ray photoelectron spectroscopy (XPS) studies, which confirmed the presence of N and Fe elements in the ATPF hydrogel (blue shaded areas in Fig. 1g, which were absent in PEGDA hydrogel). The deconvoluted XPS spectrum of the carbon region showed the presence of O═C–O (~288.5 ev, from Alg-NHS), O═C–N (~287 ev, from Alg-NHS) and C–O (~286.5 ev, from PEGDA) in the hydrogel network. Meanwhile, the presence of TA in the hydrogel was confirmed by pi-pi* interactions visible in the region of 291.8 ev (Fig. 1h). Nitrogen XPS further demonstrated the presence of NHS in both AP hydrogel and APTF hydrogel (Fig. S1).

2.3. Physical properties of APTF hydrogel

Since PEGDA forms the primary skeleton of the APTF hydrogel, it is important to understand the interactions between TA and PEGDA along with the role of Fe^{3+} in controlling the crosslinking of the hydrogel. Fig. 2a shows that the TA-crosslinked PEGDA hydrogel formed without Fe^{3+} underwent nonhomogeneous crosslinking, resulting in swelling in some portions of the PEGDA/TA hydrogels. This could be due to the diffusion-governed crosslinking, during which the surface of PEGDA had a higher crosslinking density than the bulk interior portion, leading to the formation of an inhomogeneous crosslinked network. Interestingly, this effect was eliminated by adding Fe^{3+}, which may decrease the crosslinking between TA and PEGDA as it underwent mono-chelation

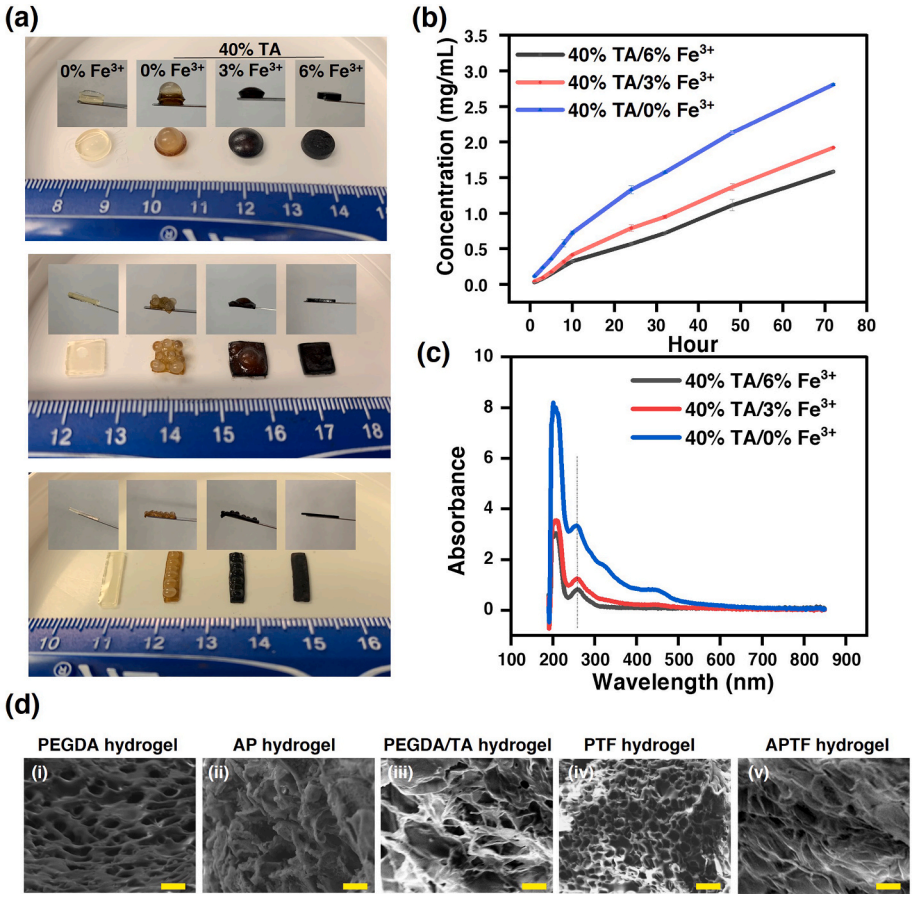

Fig. 2. Physical characterizations of PEGDA, PEGDA/TA, AP, PTF, Alg-NHS/PEGDA hydrogel treated with TA (APT) and APTF hydrogel. **(a)** Macroscopic images of PEGDA hydrogels crosslinked with TA (40%), and TA/Fe^{3+} with varied Fe^{3+} concentrations (3%, 6%). **(b)** Releasing profile of TA from PEGDA/TA or PTF hydrogels with varied Fe^{3+} concentrations. **(c)** UV–Vis of released TA from PEGDA/TA or PTF hydrogels. **(d)** Representative SEM images of the **(i)** PEGDA, **(ii)** AP, **(iii)** PEGDA/TA, **(iv)** PTF and **(v)** APTF hydrogel. Scar bar = 10 μm.

with TA. Indeed, as shown in Fig. S2, increasing the concentration of Fe^{3+} led to a decreased amount of TA crosslinked into the hydrogel network due to the blocking of H-bonds between PEGDA and TA. Hydrogels composed of PEGDA/TA/Fe^{3+} are denoted as PTF hydrogels.

Meanwhile, physically encapsulating Alg-NHS in hydrogle network inhibited nonhomogeneous crosslinking as Alg-NHS possessed fewer interactions with TA as compared to PEGDA. TA mainly interacted with PEGDA and had minimal interactions with Alg-NHS, which was confirmed by increasing the Alg-NHS concentration in the AP hydrogel (at a fixed total polymer concentration of 22%) leading to a decreased amount of TA incorporated into the hydrogel during crosslinking (Fig. S2). By interlocking the PEGDA polymer chains with Alg-NHS, a more homogeneous crosslinking was achieved, as shown in Fig. S3.

Since TA was incorporated into the hydrogel through non-covalent interactions, a release study of TA was performed over time. Although numerous studies have focused on TA-crosslinked hydrogels, only few studies reported the release kinetics of TA over time [6]. As the TA leaching may be beneficial due to its antibacterial, antioxidant, and anti-inflammatory effects [74,75], it has been used as a releasing agent for accelerating wound healing. For example, Neethu et al. developed a pH-sensitive hydrogel for sustained delivery of TA to promote wound healing [76]. However, a localized high TA concentration (>3 mg/ml) showed slight cytotoxic effects [77]. As a result, controlling the release of TA is critical for successfully executing its function in a proper manner. Fig. 2b–c and S4 demonstrate the release profiles of TA from the engineered hydrogels, formed under different treatments (40% TA/0%, 3%, 6% Fe^{3+}), over time. The decreased amount of TA leaching upon Fe^{3+}-assisted crosslinking was due to 1) less TA incorporation in the hydrogel as a result of chelation between Fe^{3+} and TA which blocked the H-bonding interactions between TA and PEGDA during crosslinking, and 2) the conversion of the mono-chelated TA/Fe^{3+} within the hydrogel to tris-chelated upon exposure to physiological pH. This pH-sensitive nature of the chelation between TA and Fe^{3+} may serve to stabilize TA within the hydrogel network [78]. Therefore, the release profile of the proposed TA/Fe^{3+} crosslinked hydrogel is highly desirable and controllable. The morphologies of different hydrogel compositions were characterized by scanning electron microscope (SEM). As shown in Fig. 2d, the pure PEGDA hydrogel (Fig. 2d–i) had the largest pore size compared with the other hydrogel compositions, presumably due to the lower crosslinking density. Interestingly, when the PEGDA hydrogel was interpenetrated with Alg-NHS, the morphology completely changed (Fig. 2d–ii). The effect of Fe^{3+} in contributing to homogenous crosslinking was also manifested in the SEM images, as the PEGDA/TA hydrogel (Fig. 2d–iii) demonstrated a larger pore size distribution compared with that of the PTF hydrogel (Fig. 2d–iv). The final APTF hydrogel demonstrated a more crosslinked structure with the highest roughness and less pores when compared to other hydrogels (Fig. 2d–v).

2.4. Mechanical characterization of APTF hydrogels

Controlling intermolecular interactions and crosslinking density within the hydrogel network is the key for tuning its mechanical properties. While TA has been shown to improve the mechanical strength of hydrogels, controlling the mechanical properties of TA containing hydrogels is limited when primarily relying upon H-bonding interactions [6,79–83]. On the other hand, ion crosslinked Alg hydrogels are known for their brittleness and weak mechanical properties (with a Young's modulus of 17 kPa and ultimate strain of 20%) [84], significantly limiting their applications as bioadhesive due to their cohesive failure during application. To address this limitation, Jeong-Yun et al. prepared a Ca-alginate/polyacrylamide (PAAm) hybrid hydrogel, through forming a ionically and covalently crosslinked network, with significantly strengthened toughness as compared to their parents, the alginate and polyacrylamide hydrogels [84]. Their work suggested that the fracture energy of resulting hydrogels could be greatly increased by combining weak and strong crosslinks. Here, we hypothesize that by incorporating Alg-NHS/Fe^{3+} into the TA crosslinked PEGDA hydrogel, the mechanical properties would significantly increase. The tunable properties originate from the Fe^{3+} which controls those two crosslinking systems through different interaction mechanisms with Alg-NHS and TA.

To optimize the APTF hydrogel, we explored the impact of applying different treatment methods on the mechanical properties of the resulting hydrogel. The results highlighted that it is essential to add TA and Fe^{3+} simultaneously to optimize the mechanical properties of the APTF hydrogel (Fig. 3a–d). Treating the AP hydrogel with TA first led to Alg-NHS leaching from the hydrogel network over time. This was confirmed by precipitation of the Alg-NHS in the TA solution after crosslinking using ethanol, whereas no Alg-NHS precipitated out after co-treating with the TA/Fe^{3+} solution (Fig. S5). The released Alg-NHS precipitated out due to a lack of H-bond interactions between Alg-NHS and TA, thereby reducing the crosslinking density between Alg-NHS and Fe^{3+} in the following step. On the other hand, treatment with Fe^{3+} first resulted in a crosslinked Alg-NHS/Fe^{3+} network within the AP hydrogel network. This was confirmed by limited swelling of the AP hydrogel when placed in Fe^{3+} solution as compared to Dulbecco's phosphate-buffered saline (DPBS) after 24 h (Fig. S6). However, the limited amount of Fe^{3+} crosslinked with Alg-NHS in the first step would be chelated by TA during the subsequent treatment. Considering the much higher amount of TA compared to Alg-NHS, the crosslinking density between Alg-NHS and Fe^{3+} was lower during the second treatment with TA, leading to weakened mechanical properties. This decreased crosslinking density was confirmed by the darkening of the TA solution after immersing the Alg-NHS/PEGDA/Fe^{3+} (APF) hydrogel into it, indicating chelation of TA and Fe^{3+}overtime as the TA/Fe^{3+} solution is dark in color while the TA solution is orange and clear. As such, we chose to use a TA/Fe^{3+} co-treatment for the APTF hydrogel synthesis, which resulted in the highest Young's modulus, ultimate strength, and toughness due to optimal crosslinking between Alg-NHS and Fe^{3+}.

We characterized the tunability of the hydrogel's mechanical properties, which was predominantly controlled by creation or alteration of the molecular interactions and crosslinking nature across the network. In our system, Alg-NHS interacts with Fe^{3+} through ionic interactions while Fe^{3+} chelates with TA in a pH-sensitive manner. Fe^{3+} forms bis-chelation with TA when the pH is higher than 1.7 [85]. In this work, the observed chelation was a mono-chelation as the pH of the 40% TA solution was highly acidic (pH = 1.5). This was further confirmed by ultraviolet–visible spectroscopy (UV–vis) which exhibited no characteristic bis-chelation and tris-chelation peaks around 600 nm (Fig. S7) [86]. Nanoparticle formation was not observed in the TA/Fe^{3+} complex as confirmed by transmission electron microscopy (TEM) and dynamic light scattering (DLS) studies on the 40% TA/3% Fe^{3+} solution. No nanoparticles were detected based on TEM images (Fig. S8a). As confirmed by the DLS results, the size distribution of 40% TA/3% Fe^{3+} solution showed no difference compared with that of Milli Q water, confirming the absence of any nanoparticles (Fig. S8b). Additionally, there was a strong H-bonding interaction between TA and PEGDA [6,87]. To investigate the contribution of each polymer (Alg-NHS and PEGDA) to the crosslinking, the total polymer concentration (22% (w/v)) was kept constant, while the ratio of Alg-NHS: PEGDA within the AP hydrogel was varied from 0:22, to 4:18, and 8:14, followed by treatment with 40% TA containing either 0, 3 or 6% Fe^{3+}. The effect of Fe^{3+} concentration on the three AP hydrogel compositions with different treatments was systematically examined.

As shown in Fig. 4a(i), increasing Fe^{3+} concentration led to a decrease in the Young's modulus of the PEGDA hydrogel (0:22). This was due to the decrease in H-bonding between PEGDA and TA, since the chelation between TA and Fe^{3+} proved to be the stronger interactions compared with H-bonding [88]. This decrease in Young's modulus was not observed for Alg-NHS/PEGDA at 4:18 (%) due to the crosslinking established between Alg-NHS and Fe^{3+}. This trend was made even more

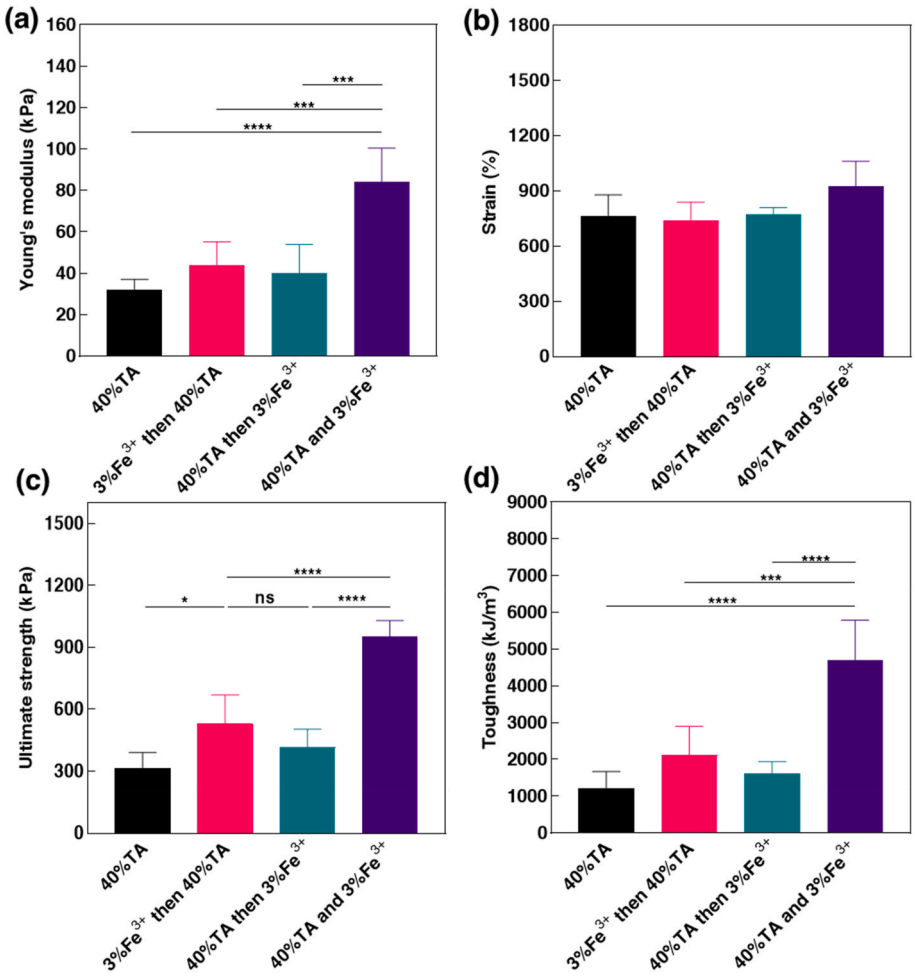

Fig. 3. Effects of treatment methods on mechanical properties of APTF hydrogel. (a) Young's modulus, **(b)** strain, **(c)** ultimate strength, and **(d)** toughness of APTF hydrogels using different treatment methods for crosslinking.

prominent upon further increasing the proportion of Alg-NHS (8:14). The same behavior was also observed for the ultimate strength and toughness of all hydrogels (Fig. 4a(ii-iii)). In fact, the chelation of Fe^{3+} with TA reduced the H-bonding interaction between TA and PEGDA, thereby lowering the stiffness. On the other hand, the interaction between Fe^{3+} and Alg-NHS could improve the mechanical properties of the resulting hydrogels. Therefore, the positive effects of increasing the Fe^{3+} concentration were more obvious when the proportion of Alg-NHS was also increased in parallel. After substituting PEGDA with Alg-NHS, the primary covalent network density decreased, which explained why the 8:14 AP hydrogel with TA/Fe^{3+} treatment demonstrated lower stiffness when compared to the 0:22 PEGDA hydrogel with TA treatment. Meanwhile, simultaneously increasing the Alg-NHS concentration and decreasing PEGDA concentration led to enriched noncovalent interactions, and an improvement in deformability with significantly improved stretchability of up to 1000% (Fig. 4a(iv)).

To understand the net effect of Alg-NHS on the mechanical properties of the hydrogel, different concentrations of Alg-NHS were added to the 22% PEGDA hydrogels which were further treated with 40% TA and 3% Fe^{3+}. Improved mechanical properties (increased ultimate strength and Young's modulus without compromising stretchability) of the hydrogels were observed with increasing Alg-NHS concentrations. This confirmed the enhanced non-covalent molecular interactions in the engineered hydrogel (Fig. 4b). The effect of PEGDA concentration on the mechanical properties of the APTF hydrogel was evaluated at constant TA (40%), Alg-NHS (8%), and Fe^{3+} (3%) concentrations. Herein, increased Young's modulus and hydrogel strength were attributed to stronger covalent interactions at higher concentration of PEGDA which could not reversibly break and heal. Therefore, due to the lack of contribution from dynamic noncovalent interactions, the stretchability of the hydrogel decreased dramatically as the PEDGA concentration was increased (Fig. 4c). Moreover, increasing Alg-NHS concentrations could increase the toughness of the hydrogels, which could not be achieved by increasing PEGDA concentrations (Fig. 4d and S9). Overall, an optimal combination of covalent and non-covalent molecular interactions inside the crosslinked network of the hydrogel provided the optimal mechanical properties.

After systematic characterization and optimization, the composition of 22% PEGDA, 8% Alg-NHS, crosslinked with 40% TA and 3% Fe^{3+} possessed the best array of desirable and broadly applicable mechanical properties for the APTF hydrogel. In this optimized hydrogel, the Young's modulus matched well with that of soft tissue (84 kPa) with a strain of 924%, an ultimate strength of 951 kPa, and a toughness of 4697 kJ/m^3, making this composition a suitable biomaterial for sealing elastic tissue (Fig. 4e–g). A representative strain-stress curve of the optimized APTF hydrogel is shown in Fig. 4e. High elasticity of APTF is shown in Fig. 4f-**g.** We further confirmed that the APTF hydrogel's strong mechanical properties, including its superb elasticity, toughness, and ultimate strength, could not be obtained in the case of a PEGDA/TA hydrogel, despite incorporating an increased PEGDA concentration (38% PEGDA crosslinked with 40% TA) (Fig. S10).

As a functional bioadhesive, it is imperative that the hydrogel maintains its structural integrity throughout the duration of application to the tissues. Most bioadhesive hydrogels lose their mechanical

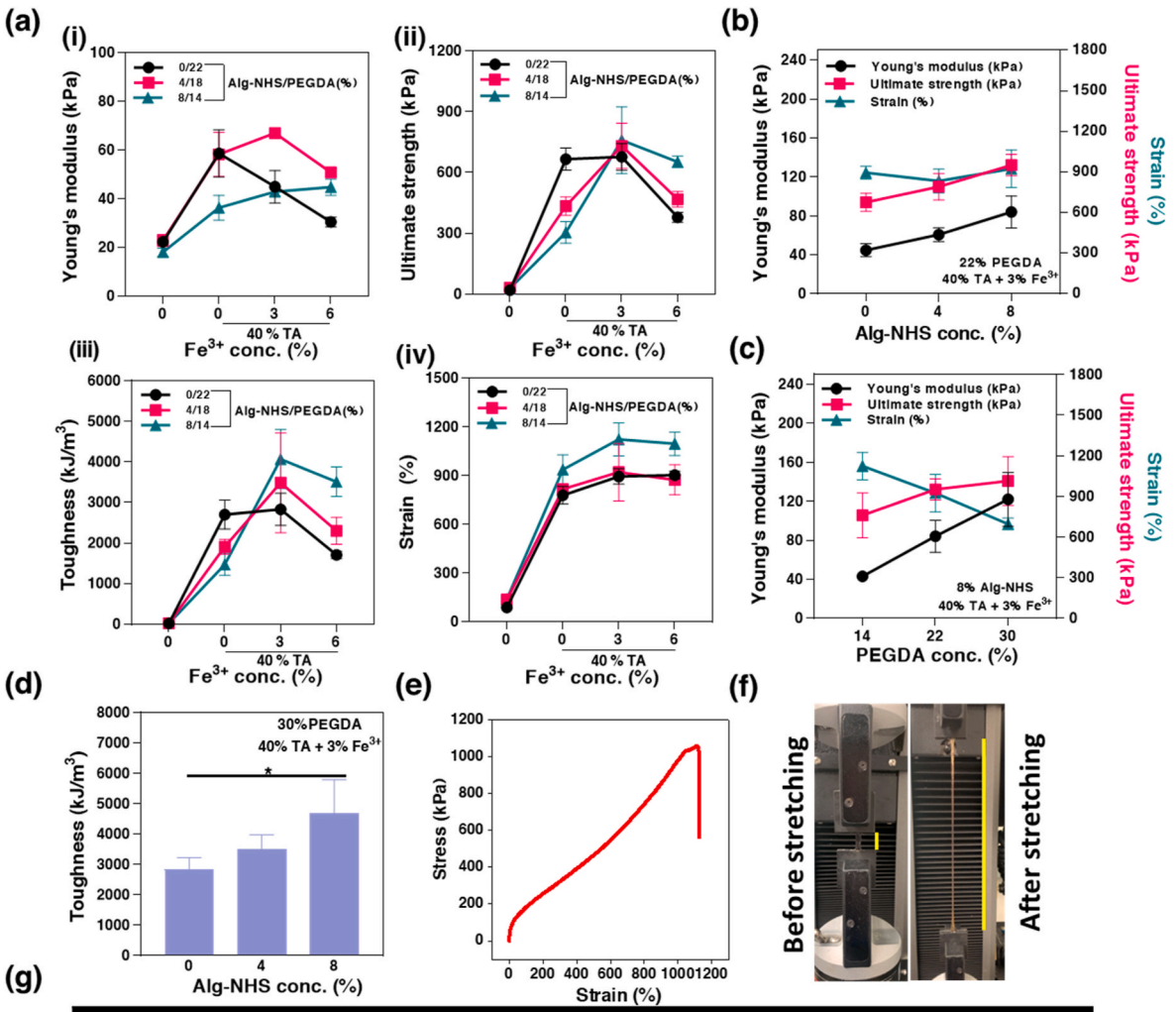

Toughness (kJ/m³)	Young's Modulus (kPa)	Strain (%)	Ultimate Strength (kPa)
4696.62 ±945.54	84.06 ±14.11	924.61 ±120.26	951.047 ±68.38

Fig. 4. Mechanical characterizations of APTF hydrogels formed by varying Alg-NHS/PEGDA ratios. (a) Mechanical properties of APTF hydrogels with fixed total polymer concentration (22%) and varied treatment methods (40% TA/0%, 3%, 6% Fe^{3+}). **(i)** Young's modulus, **(ii)** ultimate strength and **(iii)** toughness and **(iv)** ultimate strain of hydrogels treated with TA/Fe^{3+}. Young's modulus, strain, and ultimate strength of APTF hydrogels formed with varied **(b)** Alg-NHS concentrations and **(c)** PEGDA concentrations. **(d)** Toughness of APTF hydrogels with varied Alg-NHS concentrations. **(e)** Representative stress-strain curve of the optimized engineered APTF hydrogel. **(f)** Stretching of the APTF hydrogel. **(g)** Mechanical parameters of optimized APTF hydrogel.

integrity over a short period under wet conditions due to their excessive swelling [33–37], or degradation [31,32]. The mechanical stability of the APTF hydrogel was assessed in DPBS at 37 °C over time (Fig. S11). Although a drop was observed in the mechanical properties of the APTF hydrogel after 96 h, it still exhibited characteristics superior to those of the majority of freshly prepared TA-based bioadhesive hydrogels reported thus far [6,79–83], featuring values of 31 kPa Young's modulus, 798% ultimate strain, 398 kPa ultimate strength, and 1409 kJ/m^3 toughness.

2.5. Adhesive characterization of APTF hydrogel

The ability to achieve durable and rapid adhesion to the surface of wet tissue is a key requirement for the design of bioadhesives. The polyphenol-rich TA molecule is an excellent candidate for incorporation into bioadhesives due to its ability to form various interactions (e.g. chelation, H-bonding, hydrophobic interactions, Schiff base reaction, Michael type addition) with the native tissues through its five-arm structure [31,78,80,81]. The presence of catechols/pyrogallols in TA, the primary moieties in muscle foot proteins (mfps) of marine mussels to provide wet adhesion underwater, attributes enhanced tissue adherence. Initially, TA interacts with the tissue through H-bonding. Subsequently, covalent interactions with the tissue (i.e., Michael addition, Schiff base reactions) come into play after catechol moieties in TA undergoes auto-oxidization overtime to form quinones [29,89,90]. These covalent interactions provide durable adhesion of the material to the tissues during their physiological function. An ideal adhesive biomaterial should be functionalized with binding moieties that can spontaneously form both covalent and noncovalent interactions with the tissue surfaces while conforming to deformation. Adhesive moieties that have demonstrated high reactivity and spontaneous covalent interactions with tissue surfaces include aldehyde [91–94], *N*-hydroxysuccinimide (NHS) ester [1,12,72,73], isocyanates [95,96], and aryl azides [97].

We demonstrated that the APTF hydrogel exhibited strong tissue adhesion, in which NHS and TA jointly acted to form robust and instant covalent and non-covalent bonds with the tissue surfaces (Fig. 5a). Many

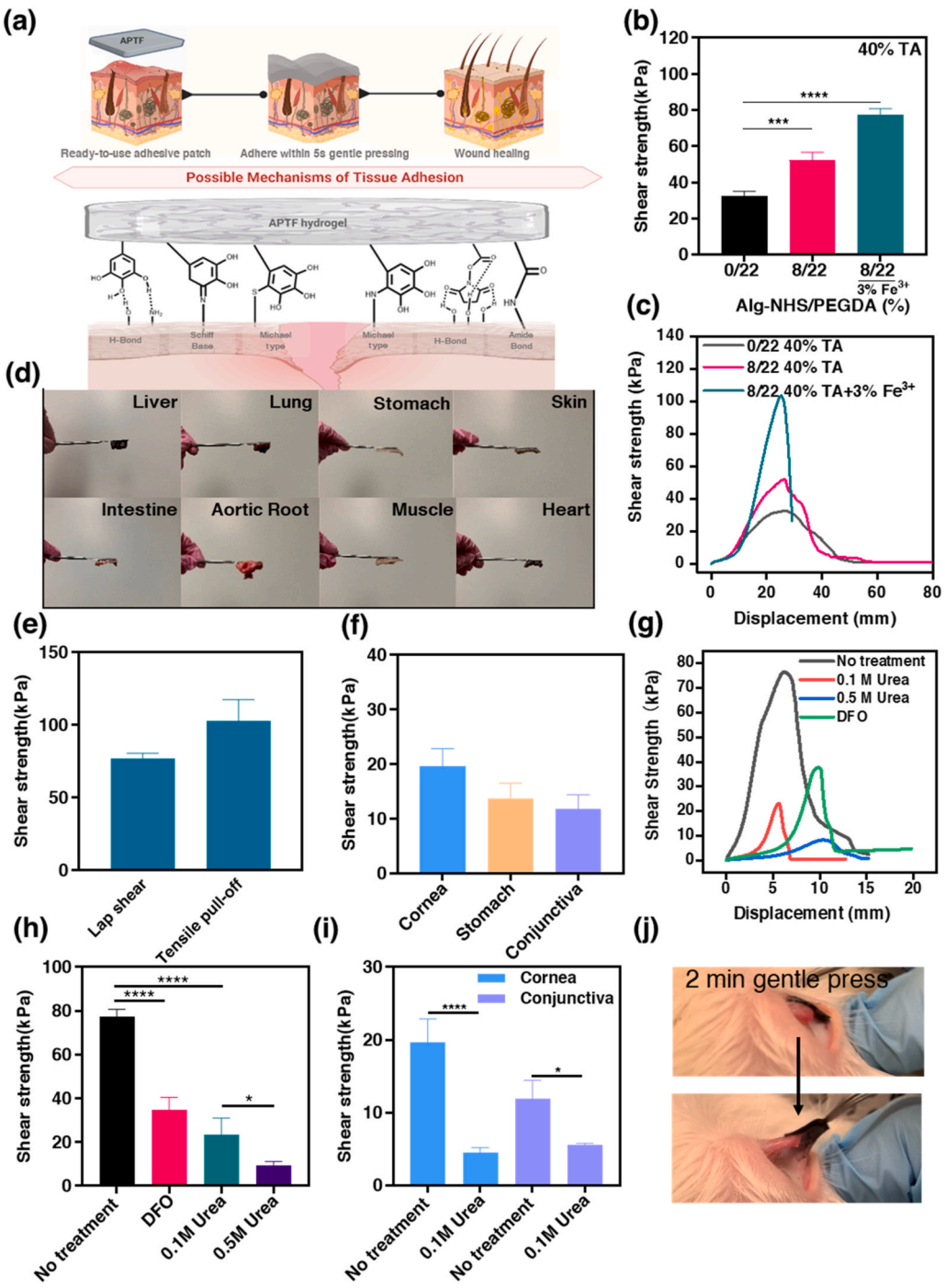

Fig. 5. Adhesion assessment of APTF hydrogels. (a) Illustration of adhesion mechanism to wet tissue surfaces. **(b)** Shear strength of different hydrogels on porcine skin and their **(c)** typical lap shear stress-strain profiles. **(d)** Demonstration of adhesiveness of APTF patch to different tissues (one side adhered to a spatula and another side adhered to tissue within 5 s gentle pressing). **(e)** Adhesive strength of APTF hydrogel using two ASTM testing methods including lap shear test and tensile pull-off test. **(f)** Shear strength of APTF hydrogel on different wet tissues. **(g)** Representative lap shear stress-strain curve and **(h)** shear strength of APTF hydrogels on porcine skin with and without urea or DFO treatment. **(i)** Shear strength of APTF hydrogels on porcine cornea and conjunctiva with and without urea treatment. **(j)** Demonstration of strong adhesion to rabbit conjunctiva *in situ*.

studies have shown compromised adhesion due to the pre-oxidation of catechol or pyrogallol prior to application [98–101], as oxidation can trigger the self-polymerization of TA by converting catechols and pyrogallols to highly reactive quinones that can react with the molecule itself rather than the tissue, thus losing the adhesive moieties [102]. Catechols start to get irreversibly oxidized, forming quinone structures when the pH is higher than 5.5 with negligible adhesion at a pH of 7.5 [102]. Marine mussels themselves have adopted a smart strategy to overcome the drop in their wet surface adhesion, caused by catechol oxidation, by generating an isolated acidic environment secluded from seawater and secreting the thiol-rich mfp-6 as a reducing agent [103–107]. Our system was designed in a similar fashion, as the APTF hydrogel was formed in an acidic pH environment that prevented the catechol/pyrogallol from undergoing oxidation, thus preserving its strong adhesiveness. American Society for Testing and Materials (ASTM) standard lap shear test (ASTM F2255) was conducted on freshly cut porcine skin tissue to quantify the adhesion efficacy of the engineered APTF hydrogel patch. At a fixed total polymer concentration (22%) with co-treatment of 40% TA and 3% Fe^{3+}, increasing Alg-NHS concentration had no effect on the adhesive strength. This was due to lower TA incorporation when less PEGDA was used (Fig. S12).

While previously reported PEGDA hydrogels showed no adherence to tissue surfaces due to their nonadhesive nature toward cells and proteins [108], treatment of PEGDA with TA enhanced the adhesive strength of the PEGDA/TA hydrogel to 32.5 ± 2.05 kPa. Herein, TA molecules with multiple hydroxyl groups interact with the polar

functionalities of the tissue surface to facilitate adhesion. The contribution of Alg-NHS to tissue adherence was demonstrated by comparing PEGDA and AP hydrogels following TA treatment. The presence of Alg-NHS increased the adhesion strength significantly from 32.5 ± 2.05 kPa for the PEGDA/TA hydrogel to 52.24 ± 3.86 kPa for the APT hydrogel due to the introduction of NHS-mediated covalent and non-covalent interactions (Fig. 5b). Meanwhile, the incorporation of Fe^{3+} into the AP hydrogel, which crosslinked the Alg-NHS moieties within the hydrogel, further improved the adhesive strength to 77.28 kPa ± 3.03 kPa by preventing the leaching of Alg-NHS from the hydrogel during crosslinking. Fig. 5c represents the shear strength-displacement curves related to the engineered hydrogels, reflecting the origin of adhesion from TA and Alg-NHS. Additionally, we found that some NHS groups could undergo acid-triggered ester hydrolysis during crosslinking, which is a reversible [109] and temperature dependent reaction [110]. The hydrolysis of NHS in the TA solution was characterized by ^{1}H NMR (Fig. S13) which showed that part of the NHS ester was hydrolyzed during the crosslinking step. This opens up possibilities for optimizing the solvent and temperature during crosslinking in the future. Quick adherence after 5 s of gentle pressing on different types of wet tissues (e.g., liver, lung, stomach, heart, muscle, and others) was assessed with the engineered APTF hydrogel and presented in Fig. 5d. One side of the patch was adhered to a spatula, while the other side was adhered to the wet tissue (Video S1). To evaluate the bonding effect of the APTF hydrogel, we further characterized the adhesiveness of the APTF hydrogel through a tensile pull-off test (ASTM F2258). As shown in Fig. 5e, the APTF hydrogel exhibited an adhesive strength of 77.28 ± 3.39 kPa based on the lap shear test and 102.8 ± 3.39 kPa based on the tensile pull-off test, which were significantly higher than that of commercial glues including Coseal, DuraSeal, Histoacryl, BioGlue, and Tisseel (less than 40 kPa) [1]. Additionally, the adhesive strength of APTF hydrogel was also higher than most of the recently developed bioadhesives [38,55,111,112]. The APTF bioadhesive also exhibited strong adhesion to a wide range of wet tissue surfaces including stomach (13.72 ± 2.81 kPa), cornea (19.61 ± 3.26 kPa), and conjunctiva (11.87 ± 2.57 kPa) (Fig. 5f).

Supplementary video related to this article can be found at https://doi.org/10.1016/j.bioactmat.2023.06.007

Removal of patches from wounds is difficult due to the risk of secondary injury and bleeding [113]. Especially for infants and diabetic patients with fragile and sensitive skin, extra-strong adhesion might exacerbate pain and cause trauma and inflammation upon removal [114]. In addition, on-demand detachment of bioadhesives is crucial for repositioning misplaced bioadhesives or for retrieving implants [50]. Achieving tough adhesion and benign triggerable detachment remains a challenge. For instance, many recently developed bioadhesives required harsh triggering conditions which are incompatible for the adjacent native tissues such as concentrated metallic ions, pH, UV irradiation, or electrical stimulus to induce the detachment [115–118]. Recently, Jiang et al. developed a gelatin-based bioadhesive that could be removed by applying cold water. However, their hydrogel suffered from low adhesive strength (less than 10 kPa) [62]. Since APTF hydrogel possesses strong adhesive properties, therefore, endowing APTF hydrogel with a chemically tunable debonding characteristic is imperative. Herein, the debonding capability of the engineered APTF patch is demonstrated in Fig. 5g and h which reveals facile patch removal upon the application of deferoxamine mesylate (DFO) and urea solutions at different concentrations. As a strong medical Fe^{3+} chelator, DFO is FDA approved and widely used in clinical cases of acute iron intoxication [119]. It has been shown that DFO readily interacted with Fe^{3+} ions involved in the crosslinking of hydrogels, leading to the resulting dissociation of the hydrogel [7]. Therefore, DFO is expected to reduce the adhesion of the hydrogel by decrosslinking and subsequently decomposing the hydrogel network. Meanwhile, urea is a naturally occurring molecule, which is produced during protein metabolism and present in large amounts in human blood and urine [120,121]. Urea molecules have a superior tendency to form hydrogen bonds and can thus interact with interfacial TA molecules to weaken the adhesion of the hydrogel patch to the tissue surface [6]. Here, we showed that using a higher concentration of urea significantly lowered the adhesion strength of the patch (Fig. 5h). The on-demand detachment characteristics were also assessed using wet tissues such as the cornea and conjunctiva. As is shown in Fig. 5i, the application of 50 μL urea (0.1 M) could significantly reduce the adhesion to the tissue substrates. As the required concentrations and amounts of the urea and DFO for detachment were remarkably lower than their safe dosage used in clinics [121–125], we do not expect to see any side effects with using them.

To demonstrate handling and clinical application of the designed material, tissue adhesion was tested *in situ* using a rabbit eye conjunctiva and pig cornea. Cornea and conjunctiva were adopted to assess the wet adhesion of the designed APTF hydrogel since these tissues are known for their consistent secretion of tear fluid and mucin, which lubricate the eye but limit surface adhesion [126]. To the best of our knowledge, there is no ready-to-use bioadhesive patch developed for quick adherence to the eye due to its slippery and extremely wet surface. To demonstrate the potential *in vivo* wet adhesion of the APTF bioadhesive to the cornea and conjunctiva, adhesion was assessed immediately after euthanizing the rabbit and pig when the cornea and conjunctiva surfaces were fresh and wet. We demonstrated that the APTF patch strongly adhered to the eye conjunctiva upon gentle pressing for 1 min, and the wet adhesion was immediately assessed by attempting to remove the patch with a tweezer (Fig. 5j). Further, in addition to the demonstration of robust adhesion, the painless on-demand detachment of the APTF hydrogel was also shown by applying 2–3 drops of a 0.1 M urea solution to the adhesion site in both animal models (Video S2 and S3).

Supplementary video related to this article can be found at https://doi.org/10.1016/j.bioactmat.2023.06.007

2.6. *In vitro* biocompatibility assay of APTF hydrogel

To evaluate the biocompatibility of the APTF hydrogel, 3T3 cells were drop-seeded on top of the AP and APTF hydrogels, followed by incubation for 7 days. NIH 3T3 fibroblasts were selected because it is one of the most frequently used cell lines for studying biomaterial biocompatibility and cytotoxicity in accordance with the International Organization for Standardization (ISO) norm 10993-5 [127–130]. A live/dead assay demonstrated excellent cellular viability (>90%) for both AP and APTF hydrogels up to 7 days post-seeding (Fig. 6a–b, S14). Fluorescent F-actin/cell nuclei staining was also performed to demonstrate cell proliferation and spreading on hydrogels up to 7 days post-seeding (Fig. S15). However, due to the lack of arginine-glycine-aspartic acid (RGD) moieties in the hydrogel, the cells proliferated relatively slowly on both the AP and APTF hydrogels as demonstrated by a PrestoBlue assay (Fig. 6c). To further evaluate the biocompatibility of the APTF hydrogel, we cultured NIH 3T3 cells in Transwell® cell culture inserts and exposed them to APTF hydrogel. In this experiment, NIH 3T3 cells were seeded at the bottom of a 24-wells Transwell permeable (Costar®, 8 μm PET membrane) at a cell density of 2×10^4 cells/cm^2. APTF hydrogels were placed into Transwell inserts, and 1 mL of growth medium (Dulbecco's Modified Eagle's Medium) was added to each well of the Transwell permeable supports. As shown in Fig. S16, based on a live/dead assay, cells treated with APTF hydrogel showed no difference compared with that of the control group, confirming the *in vitro* biocompatibility of the APTF hydrogel.

2.7. Antioxidant activities of APTF hydrogel

Free radicals generated at the wound site may cause oxidative stress and cytotoxicity by damaging DNA and enzymes [131]. Antioxidant bioadhesive patches can facilitate the wound healing process by scavenging excess reactive oxygen species (ROS). The antioxidant properties of the APTF patches were determined by evaluating the scavenging

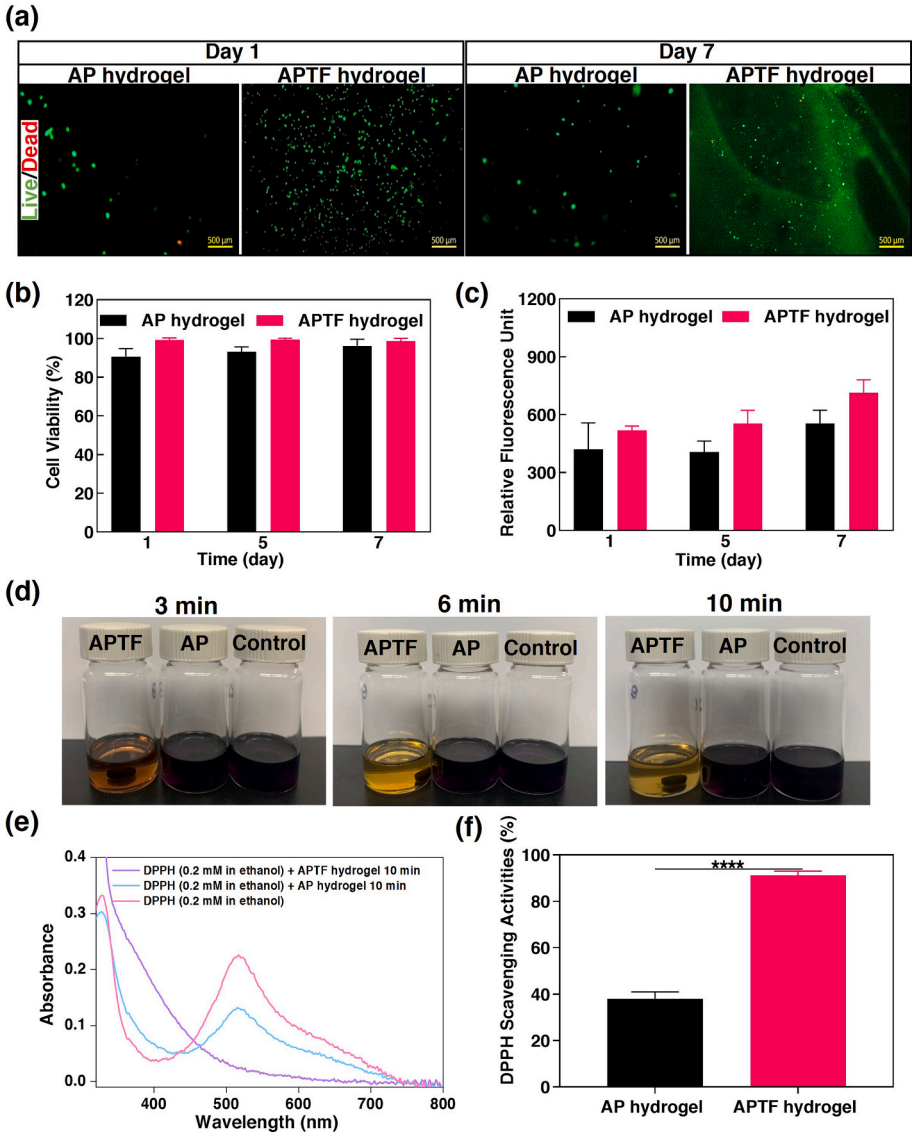

Fig. 6. *In vitro* biocompatibility and antioxidant activity of APTF hydrogel. *In vitro* cell studies: **(a)** Representative live/dead stained images of 3T3 cells on AP hydrogel and APTF hydrogel on day 1 and day 7. **(b)** Quantification of cellular viability for 3T3 cells seeded on AP and APTF hydrogel over 7 days of culture. **(c)** Cellular proliferation on AP hydrogel and APTF hydrogel over time based on PrestoBlue assay. *In vitro* antioxidant activity: **(d)** The color changes of the three DPPH• solutions containing hydrogel-lacking control, AP hydrogel, APTF hydrogel over time. **(e)** Absorbance change of DPPH• before and after the reaction. **(f)** The DPPH• scavenging activities of AP and APTF hydrogels.

ability of the hydrogels against the stable free radical colorimetric probe, 1,1-diphenyl-2-picrylhydrazine (DPPH•), where the color change can be quantified by UV–vis spectrophotometry [132]. TA is known to have antimutagenic and antioxidant activities. The antioxidant activity of TA is attributed to its capacity to form a complex with ferric ions, interfering with the Fenton reaction [133]. Here, to evaluate the antioxidant properties of the engineered hydrogels, the color changes of the three DPPH• solutions exposed to the hydrogel-lacking control, the AP hydrogel and the APTF hydrogel were monitored at different time points. As shown in Fig. 6d, the color of the DPPH• solution exposed to the APTF hydrogel changed from dark purple to light yellow within 10 min, which was not observed in DPPH• solutions exposed to either the hydrogel-lacking control or the AP hydrogel. Typically, DPPH radicals gave a strong absorption at 517 nm in the UV visible spectroscopy. After being reduced, the strong peak at 517 nm disappeared only in the case of the APTF hydrogel (Fig. 6e). We found that the APTF hydrogel possessed strong antioxidant activities with 91% radical scavenging efficiency due to the presence of TA/Fe^{3+} complexes (Fig. 6f).

2.8. Photothermal properties and near-infrared (NIR)-assisted antimicrobial activity of APTF hydrogel

Photothermal ablation, which utilizes photothermal agents under NIR radiation (700 nm–1400 nm), has been applied to kill antibiotic-resistant bacteria in the treatment of infections [134]. Consequently, mild photothermal ablation has received significant attention as an alternative treatment to conventional antibiotics due to its remote deep tissue penetration to kill bacteria without damaging normal tissues. On the other hand, compared to traditional photothermal agents such as Au nanoparticles, the hydrogel compound consisting of catechol-Fe^{3+} can protect normal tissues from thermal damage while mitigating adverse effects such as nanomaterial diffusion [68].

Therefore, we envision that the APTF hydrogel containing TA/Fe^{3+} can effectively absorb and convert NIR light to heat for antibacterial applications. To test this, an 808 nm NIR laser was used to characterize the photothermal properties of the APTF hydrogel under wet and dry conditions. After irradiation for 4 min, the temperature increments of a dry APTF hydrogel were 27.6 °C and 38.6 °C at 0.015 W/cm^2 and 0.016 W/cm^2, respectively (Fig. 7a). For a wet APTF hydrogel, the temperature dropped to 22.53 °C at 0.015 W/cm^2, and 37.8 °C at 0.016 W/cm^2 (Fig. 7b). However, the pure AP hydrogel showed almost no temperature increase at 0.016 W/cm^2 in either dry or wet conditions (~5 °C and ~0 °C), indicating a lack of photothermal effects. Meanwhile, pyrogallol-Fe^{3+} crosslinked APTF displayed a tunable photothermal capacity, depending on the intensity of NIR light exposed to the hydrogel surface. A cyclic photothermal heating test demonstrated that the APTF hydrogel

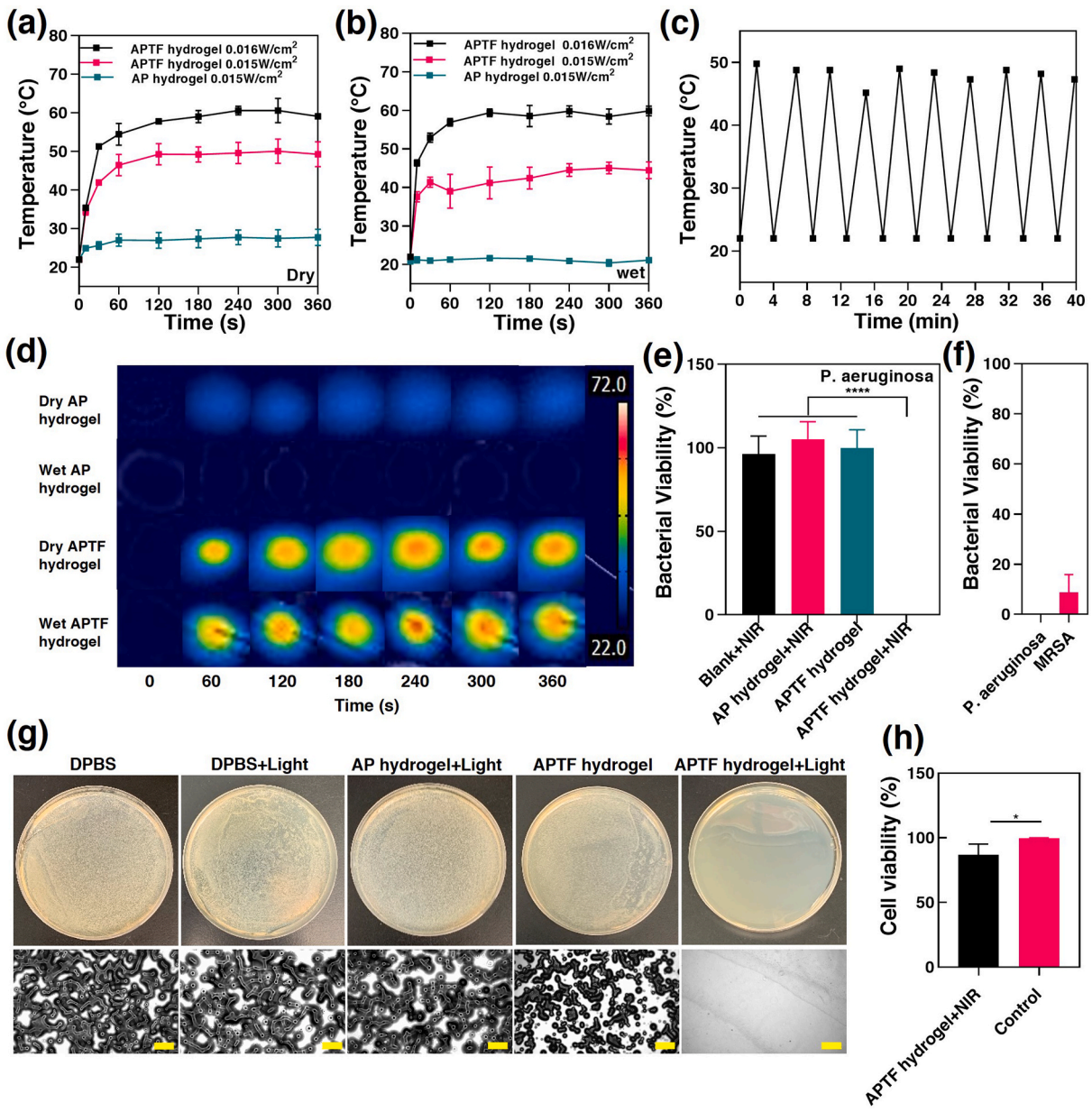

Fig. 7. Photothermal and antibacterial properties of the APTF hydrogels. Temperature enhancement over time for the **(a)** dry APTF hydrogels and **(b)** wet APTF hydrogels under irradiation with a NIR laser (808 nm) under different power densities. **(c)** Photothermal stability of the engineered APTF hydrogel undergoing 10 consecutive heating cycles. **(d)** Infrared thermal images of the AP and APTF hydrogels under 808 nm irradiation for 6 min. **(e)** Quantitative antibacterial efficiency against *p. aeruginosa* under different treatment conditions. **(f)** Quantitative antibacterial efficiency of APTF hydrogel against *p. aeruginosa* and MRSA under 808 nm irradiation. **(g)** Representative images from the *p. aeruginosa* colonies on the agar plates after treatment with DPBS, DPBS + light, AP hydrogel + light, APTF hydrogel, APTF hydrogel + light. Images were taken from a Zeiss Axio Observer Z1 inverted microscope. Scar bar = 500 μm. **(h)** Cell viability in the presence of APTF hydrogel after 5 min irradiation.

could be heated to 50 °C in 2 min during irradiation. Upon removal of irradiation, the APTF hydrogel could cool down to room temperature within 2 min. The application of 10 consecutive heating cycles demonstrated the photothermal stability of the APTF hydrogel, indicating no long-term degradative photothermal effects (Fig. 7c). Moreover, the infrared images showed that the maximum photothermal temperature of the APTF hydrogels was quickly reached in 1 min and remained stable over 5 min, confirming the practical usability of the hydrogel in both dry and wet conditions (Fig. 7d).

Our APTF hydrogel demonstrated NIR-assisted antibacterial functionality because the hydrogel reached and exceeded a photothermal temperature of 45 °C, beyond which the viability of some bacterial enzymes begins to rapidly decline due to denaturation, resulting in bacterial death [7,135]. The NIR-assisted antibacterial property of APTF hydrogels was then assessed against Pseudomonas aeruginosa (*P. aeruginosa*) and Methicillin-resistant staphylococcus aureus (MRSA). After irradiation for 5 min, each survived bacteria sample was seeded with a 1 mL aliquot of DPBS solution. After an additional 5 min, bacteria samples were spread onto agar plate, incubated overnight, and the colonies were counted. Our results revealed nearly complete eradication of *P. aeruginosa* when the NIR assisted APTF hydrogel was used with a log reduction of 5.389. Meanwhile, NIR light alone provided no bactericidal effects. Among the tested samples, only the combination of the APTF hydrogel assisted with NIR light interacted synergistically to demonstrate antimicrobial activity whereas the APTF hydrogel without NIR light assistance showed no difference in bacterial viability compared to

the control (Fig. 7e and g). In addition, the AP hydrogel with NIR light also showed zero antibacterial activity. The strong antibacterial properties of APTF hydrogel were confirmed against both gram positive bacteria (MRSA) with only 8.733 ± 7.12% bacterial viability and gram negative (*P. aeruginosa*) bacteria with complete eradication (Fig. 7f), presumably because Staphylococcus aureus can tolerate higher temperatures when compared with other bacteria [136]. Having potent effects for killing bacterial without causing cellular toxicity is important for the safe usage of APTF bioadhesive for medical applications. Compared with the control group (cells without any treatment), the APTF hydrogel coupled with NIR had a mild cytotoxic effect on 3T3 cell viability (Fig. 7h and S17). In general, sustained exposure to high temperatures (above 50 °C) may cause irreversible damage to normal cells and tissues [137,138], while heat-induced cell death (e.g., apoptosis) at lower temperatures (42–47 °C) can be reversed with the help of heat shock proteins [139,140]. The optimal temperature for enzymatic activity in bacteria is between 30 and 40 °C and is strongly inhibited at higher temperatures [7,141–143]. Therefore, careful control of irradiation intensity and time is crucial to avoid the side effects of NIR laser on normal cells and tissues while killing bacteria. In one study, Lee et al. developed a hydrogel platform that was photopolymerized through NIR light irradiation for cell delivery. After a 5 min incubation at 45 °C, 3T3 cell viability around 86% was observed, which was comparable to the cells incubated at 37 °C [144]. In fact, many studies have shown that a temperature of 40–50 °C can effectively kill bacteria without causing any damage to the cells [143,145]. When the temperature was higher than 50 °C, strong bacterial killing effects were observed (>90% killing efficiency) with mild or partial cell damage, and these cells could rapidly proliferate to a normal state [146–148]. In another study, Li et al. developed a TA/Fe^{3+}-based hydrogel for NIR-assisted antibacterial wound treatment. The hydrogel could reach a temperature of more than 60 °C that efficiently killed *S. aureus* and *E. coli* (>90% killing efficiency). A certain extent of apoptosis of the fibroblasts was detected. However, fibroblasts around the treated site could rapidly proliferate and reach almost the same number as the control group after irradiation [149].

In our study, we used a FLIR thermal camera to record the temperature of both sides of the hydrogel during application. We found that although the surface of the hydrogel (~1 mm thickness) facing the light could reach a temperature of 60 °C after 5 min irradiation, the back side of the hydrogel, interfacing directly with cells, could achieve slightly above 40 °C, ensuring its safe usage (Fig. S18). In a recent work where catechol–Fe^{3+} was adopted for NIR-assisted antibacterial purposes, it was reported that the wound site temperature of the hydrogel group could increase to above 50 °C within 3 min in an *in vivo* infected skin wound, while the tissue around the hydrogel just showed a slight temperature increase to about 38 °C, and the temperature of other parts of the mouse had no significant change [150]. Due to its minimal interaction with living tissue and ability to kill bacteria without causing serious damage to cells, NIR light has been combined with various biomaterials and used for different medical applications. This was demonstrated in a variety of reported *in vivo* wound healing models, where NIR-assisted therapy showed the best wound healing outcomes with the least inflammation, best regenerative results, and no tissue damage compared to other groups with no NIR treatment [7,143,145,147–149,151–158]. Our results together suggest that APTF hydrogel can provide antibacterial effects with no significant damage on cells.

3. Conclusion

We have demonstrated the development of a multifunctional bioadhesive with selectively tunable physical properties for the sealing and treatment of injured tissues. The engineered bioadhesive hydrogel was formed *via* a combination of Alg-NHS, PEGDA, TA and Fe^{3+}. By fine-tuning the covalent and noncovalent molecular interactions within the hydrogel network, the resulting APTF hydrogel demonstrated excellent toughness, appropriate stiffness, and improved ultimate strength and elasticity without any tradeoffs. Long-term mechanical integrity was also well-preserved under wet conditions. In addition, robust and instant adhesion was achieved through the synergistic effects of dual adhesive moieties (NHS and TA) in the hydrogel, governing the tissue-material interfacial interactions. We also demonstrated the on-demand removal of the designed adhesive patch through the direct application of nontoxic agents to the tissue-material interfaces. Meanwhile, the presence of TA/Fe^{3+} imparted multiple functionalities to the hydrogel system, including antibacterial and antioxidant properties suitable for wound healing. Additionally, the hydrogel demonstrated excellent *in vitro* biocompatibility. This work showcases the tunability of a single hydrogel platform with unique physio-chemical characteristics, including superior mechanical, adhesive properties, along with multifunctionalities (i.e., antioxidant and antibacterial effects), making it suitable for the clinical treatment of wounds across diverse tissue types. Furthermore, this biomaterial platform opens new avenues for the design and molecular engineering of bioadhesive hydrogels for various biomedical applications.. Our future work will focus on assessing the *in vivo* biocompatibility and wound healing effects of the engineered APTF hydrogel using different animal models to broaden its application as bioadhesives for wound sealing and repair, hemostatic patches for hemorrhage control as well as matrices for drug delivery.

4. Materials and methods

The detailed experimental methods can be found in the Supplemental Information file.

Ethics approval and consent to participate

Nothing to report.

Declaration of competing interest

The authors declare no conflict of interests.

CRediT authorship contribution statement

Yuting Zheng: Conceptualization, Methodology, Validation, Formal analysis, Investigation, Data curation, Writing – original draft, Writing – review & editing, Visualization. **Avijit Baidya:** Writing – review & editing, Visualization. **Nasim Annabi:** Writing – review & editing, Visualization, Supervision, Project administration, Funding acquisition.

Acknowledgements

We acknowledge Kaavian Shariati for helping with proofreading the manuscript and his contribution to the cover. We acknowledge the support from the National Institutes of Health (R01-EB023052; R01HL140618). We acknowledge Biorender.com for helping with schematic illustration.

Appendix A. Supplementary data

Supplementary data to this article can be found online at https://doi.org/10.1016/j.bioactmat.2023.06.007.

References

[1] H. Yuk, C.E. Varela, C.S. Nabzdyk, X. Mao, R.F. Padera, E.T. Roche, X. Zhao, Dry double-sided tape for adhesion of wet tissues and devices, Nature 575 (7781) (2019) 169–174.
[2] Y. Gao, K. Peng, S. Mitragotri, Covalently crosslinked hydrogels via step-growth reactions: crosslinking chemistries, polymers, and clinical impact, Adv. Mater. 33 (25) (2021), e2006362.

[3] C. Jumelle, A. Yung, E.S. Sani, Y. Taketani, F. Gantin, L. Bourel, S. Wang, E. Yuksel, S. Seneca, N. Annabi, R. Dana, Development and characterization of a hydrogel-based adhesive patch for sealing open-globe injuries, Acta Biomater. 137 (2022) 53–63.

[4] N. Annabi, D. Rana, E. Shirzaei Sani, R. Portillo-Lara, J.L. Gifford, M.M. Fares, S. M. Mithieux, A.S. Weiss, Engineering a sprayable and elastic hydrogel adhesive with antimicrobial properties for wound healing, Biomaterials 139 (2017) 229–243.

[5] J.C. Tang, K. Xi, H. Chen, L.J. Wang, D.Y. Li, Y. Xu, T.W. Xin, L. Wu, Y.D. Zhou, J. Bian, Z.W. Cai, H.L. Yang, L.F. Deng, Y. Gu, W.G. Cui, L. Chen, Flexible osteogenic glue as an all-in-one solution to assist fracture fixation and healing, Adv. Funct. Mater. 31 (38) (2021), 2102465.

[6] K. Chen, Q. Lin, L. Wang, Z. Zhuang, Y. Zhang, D. Huang, H. Wang, An all-in-one tannic acid-containing hydrogel adhesive with high toughness, notch insensitivity, self-healability, tailorable topography, and strong, instant, and on-demand underwater adhesion, ACS Appl. Mater. Interfaces 13 (8) (2021) 9748–9761.

[7] Y. Liang, Z. Li, Y. Huang, R. Yu, B. Guo, Dual-dynamic-bond cross-linked antibacterial adhesive hydrogel sealants with on-demand removability for post-wound-closure and infected wound healing, ACS Nano 15 (4) (2021) 7078–7093.

[8] Y. Zhang, Y. Huang, Rational design of smart hydrogels for biomedical applications, Front. Chem. 8 (2020), 615665.

[9] L. Xu, C. Wang, Y. Cui, A. Li, Y. Qiao, D. Qiu, Conjoined-network rendered stiff and tough hydrogels from biogenic molecules, Sci. Adv. 5 (2) (2019), eaau3442.

[10] H. Yuk, T. Zhang, G.A. Parada, X.Y. Liu, X.H. Zhao, Skin-inspired hydrogel-elastomer hybrids with robust interfaces and functional microstructures, Nat. Commun. 7 (1) (2016) 1–11.

[11] E.S. Sani, R.P. Lara, Z. Aldawood, S.H. Bassir, D. Nguyen, A. Kantarci, G. Intini, N. Annabi, An antimicrobial dental light curable bioadhesive hydrogel for treatment of peri-implant diseases, Matter 1 (4) (2019) 926–944.

[12] B. Kong, R. Liu, Y. Cheng, Y. Shang, D. Zhang, H. Gu, Y. Zhao, W. Xu, Structural color medical patch with surface dual-properties of wet bioadhesion and slipperiness, Adv. Sci. 9 (31) (2022), e2203096.

[13] D.D. Ye, P.C. Yang, X.J. Lei, D.H. Zhang, L.B. Li, C.Y. Chang, P.C. Sun, L.N. Zhang, Robust anisotropic cellulose hydrogels fabricated via strong self-aggregation forces for cardiomyocytes unidirectional growth, Chem. Mater. 30 (15) (2018) 5175–5183.

[14] S. Choi, Y. Choi, J.J.A.F.M. Kim, Anisotropic hybrid hydrogels with superior mechanical properties reminiscent of tendons or ligaments, Adv. Funct. Mater. 29 (38) (2019), 1904342.

[15] L. Han, L.W. Yan, K.F. Wang, L.M. Fang, H.P. Zhang, Y.H. Tang, Y.H. Ding, L. T. Weng, J.L. Xu, J. Weng, Y.J. Liu, F.Z. Ren, X. Lu, Tough, self-healable and tissue-adhesive hydrogel with tunable multifunctionality, NPG Asia Mater. 9 (4) (2017) e372, e372.

[16] M.J. Lundahl, A.G. Cunha, E. Rojo, A.C. Papageorgiou, L. Rautkari, J.C. Arboleda, O.J. Rojas, Strength and water interactions of cellulose I filaments wet-spun from cellulose nanofibril hydrogels, Sci. Rep. 6 (1) (2016), 30695.

[17] X. Sun, H. Wang, Y. Ding, Y. Yao, Y. Liu, J. Tang, Fe(3+)-Coordination mediated synergistic dual-network conductive hydrogel as a sensitive and highly-stretchable strain sensor with adjustable mechanical properties, J. Mater. Chem. B 10 (9) (2022) 1442–1452.

[18] H. Lei, L. Dong, Y. Li, J. Zhang, H. Chen, J. Wu, Y. Zhang, Q. Fan, B. Xue, M. Qin, B. Chen, Y. Cao, W. Wang, Stretchable hydrogels with low hysteresis and anti-fatigue fracture based on polyprotein cross-linkers, Nat. Commun. 11 (1) (2020) 4032.

[19] A.J. Engler, S. Sen, H.L. Sweeney, D.E. Discher, Matrix elasticity directs stem cell lineage specification, Cell 126 (4) (2006) 677–689.

[20] Q. Chen, H. Chen, L. Zhu, J. Zheng, Fundamentals of double network hydrogels, J. Mater. Chem. B 3 (18) (2015) 3654–3676.

[21] A. Bin Imran, K. Esaki, H. Gotoh, T. Seki, K. Ito, Y. Sakai, Y.J.N.c. Takeoka, Extremely stretchable thermosensitive hydrogels by introducing slide-ring polyrotaxane cross-linkers and ionic groups into the polymer network, Nat. Commun. 5 (1) (2014) 1–8.

[22] C.L. McGann, E.A. Levenson, K.L. Kiick, Resilin-based hybrid hydrogels for cardiovascular tissue engineering, Macromolecules 214 (2) (2013) 203–213.

[23] D.W. Zhao, Y. Zhu, W.K. Cheng, G.W. Xu, Q.W. Wang, S.X. Liu, J. Li, C.J. Chen, H. P. Yu, L.B. Hu, A dynamic gel with reversible and tunable topological networks and performances, Matter 2 (2) (2020) 390–403.

[24] T. Huang, H.G. Xu, K.X. Jiao, L.P. Zhu, H.R. Brown, H.L. Wang, A novel hydrogel with high mechanical strength: a macromolecular microsphere composite hydrogel, Adv. Mater. 19 (12) (2007) 1622–+.

[25] Y. Zheng, K. Huang, X. You, B. Huang, J. Wu, Z. Gu, Hybrid hydrogels with high strength and biocompatibility for bone regeneration, Int. J. Biol. Macromol. 104 (Pt A) (2017) 1143–1149.

[26] D.F. Coutinho, S.V. Sant, H. Shin, J.T. Oliveira, M.E. Gomes, N.M. Neves, A. Khademhosseini, R.L. Reis, Modified Gellan Gum hydrogels with tunable physical and mechanical properties, Biomaterials 31 (29) (2010) 7494–7502.

[27] Q. Lin, C.J.C.C. Ke, Conductive and anti-freezing hydrogels constructed by pseudo-slide-ring networks, Chem. Commun. 58 (2) (2022) 250–253.

[28] F. Sabbagh, I.I. Muhamad, Z. Nazari, P. Mobini, N.M. Khatir, Investigation of acyclovir-loaded, acrylamide-based hydrogels for potential use as vaginal ring, Mater. Today Commun. 16 (2018) 274–280.

[29] S. Nam, D. Mooney, Polymeric tissue adhesives, Chem. Rev. 121 (18) (2021) 11336–11384.

[30] S. Park, H. Yuk, R. Zhao, Y.S. Yim, E.W. Woldeghebriel, J. Kang, A. Canales, Y. Fink, G.B. Choi, X. Zhao, P. Anikeeva, Adaptive and multifunctional hydrogel hybrid probes for long-term sensing and modulation of neural activity, Nat. Commun. 12 (1) (2021) 3435.

[31] M. Shin, J.H. Ryu, J.P. Park, K. Kim, J.W. Yang, H. Lee, DNA/Tannic acid hybrid gel exhibiting biodegradability, extensibility, tissue adhesiveness, and hemostatic ability, Adv. Funct. Mater. 25 (8) (2015) 1270–1278.

[32] K.Y. Lu, Y.C. Lin, H.T. Lu, Y.C. Ho, S.C. Weng, M.L. Tsai, F.L. Mi, A novel injectable in situ forming gel based on carboxymethyl hexanoyl chitosan/hyaluronic acid polymer blending for sustained release of berberine, Carbohydr. Polym. 206 (2019) 664–673.

[33] H. Montazerian, A. Baidya, R. Haghniaz, E. Davoodi, S. Ahadian, N. Annabi, A. Khademhosseini, P.S. Weiss, Stretchable and bioadhesive gelatin methacryloyl-based hydrogels enabled by in situ dopamine polymerization, ACS Appl. Mater. Interfaces 13 (34) (2021) 40290–40301.

[34] R. Subramani, A. Izquierdo-Alvarez, P. Bhattacharya, M. Meerts, P. Moldenaers, H. Ramon, H. Van Oosterwyck, The influence of swelling on elastic properties of polyacrylamide hydrogels, Front Mater 7 (2020) 212.

[35] B.D. Johnson, D.J. Beebe, W. Crone, Effects of swelling on the mechanical properties of a pH-sensitive hydrogel for use in microfluidic devices, Mat Sci Eng C-Bio S 24 (4) (2004) 575–581.

[36] Y. Zhuang, F. Yu, H. Chen, J. Zheng, J. Ma, J.H. Chen, Alginate/graphene double-network nanocomposite hydrogel beads with low-swelling, enhanced mechanical properties, and enhanced adsorption capacity, J. Mater. Chem. 4 (28) (2016) 10885–10892.

[37] H. Kamata, Y. Akagi, Y. Kayasuga-Kariya, U.I. Chung, T. Sakai, "Nonswellable" hydrogel without mechanical hysteresis, Science 343 (6173) (2014) 873–875.

[38] Z. Yang, R. Huang, B. Zheng, W. Guo, C. Li, W. He, Y. Wei, Y. Du, H. Wang, D. Wu, H. Wang, Highly stretchable, adhesive, biocompatible, and antibacterial hydrogel dressings for wound healing, Adv. Sci. 8 (8) (2021), 2003627.

[39] S. Mantha, S. Pillai, P. Khayambashi, A. Upadhyay, Y. Zhang, O. Tao, H.M. Pham, S.D. Tran, Smart hydrogels in tissue engineering and regenerative medicine, Materials 12 (20) (2019) 3323.

[40] H. Yuk, B. Lu, X. Zhao, Hydrogel bioelectronics, Chem. Soc. Rev. 48 (6) (2019) 1642–1667.

[41] J. Li, A.D. Celiz, J. Yang, Q. Yang, I. Wamala, W. Whyte, B.R. Seo, N.V. Vasilyev, J.J. Vlassak, Z. Suo, D.J. Mooney, Tough adhesives for diverse wet surfaces, Science 357 (6349) (2017) 378–381.

[42] C.E. Brubaker, P.B. Messersmith, Enzymatically degradable mussel-inspired adhesive hydrogel, Biomacromolecules 12 (12) (2011) 4326–4334.

[43] J.R. Soucy, E. Shirzaei Sani, R. Portillo Lara, D. Diaz, F. Dias, A.S. Weiss, A. N. Koppes, R.A. Koppes, N. Annabi, Photocrosslinkable gelatin/tropoelastin hydrogel adhesives for peripheral nerve repair, tissue engineering, Part A 24 (17–18) (2018) 1393–1405.

[44] X. Zhao, Q. Lang, L. Yildirimer, Z.Y. Lin, W. Cui, N. Annabi, K.W. Ng, M. R. Dokmeci, A.M. Ghaemmaghami, A. Khademhosseini, Photocrosslinkable gelatin hydrogel for epidermal tissue engineering, Adv Healthc Mater 5 (1) (2016) 108–118.

[45] Y. Hong, F. Zhou, Y. Hua, X. Zhang, C. Ni, D. Pan, Y. Zhang, D. Jiang, L. Yang, Q. Lin, Y. Zou, D. Yu, D.E. Arnot, X. Zou, L. Zhu, S. Zhang, H. Ouyang, A strongly adhesive hemostatic hydrogel for the repair of arterial and heart bleeds, Nat. Commun. 10 (1) (2019) 2060.

[46] O. Jeon, J.E. Samorezov, E. Alsberg, Single and dual crosslinked oxidized methacrylated alginate/PEG hydrogels for bioadhesive applications, Acta Biomater. 10 (1) (2014) 47–55.

[47] H. Chopra, S. Kumar, I. Singh, Bioadhesive hydrogels and their applications, Bioadhesives in Drug Delivery (2020) 147–170.

[48] Y.G. Shi, D. Li, J.F. Ding, C.L. He, X.S. Chen, Physiologically relevant pH- and temperature-responsive polypeptide hydrogels with adhesive properties, Polym Chem-Uk 12 (19) (2021) 2832–2839.

[49] D. Zhou, S. Li, M. Pei, H. Yang, S. Gu, Y. Tao, D. Ye, Y. Zhou, W. Xu, P. Xiao, Dopamine-modified hyaluronic acid hydrogel adhesives with fast-forming and high tissue adhesion, ACS Appl. Mater. Interfaces 12 (16) (2020) 18225–18234.

[50] N. Annabi, K. Yue, A. Tamayol, A. Khademhosseini, Elastic sealants for surgical applications, Eur. J. Pharm. Biopharm. 95 (Pt A) (2015) 27–39.

[51] L. Han, X. Lu, M. Wang, D. Gan, W. Deng, K. Wang, L. Fang, K. Liu, C.W. Chan, Y. J.S. Tang, A mussel-inspired conductive, self-adhesive, and self-healable tough hydrogel as cell stimulators and implantable bioelectronics, Small 13 (2) (2017), 1601916.

[52] J. Jing, S. Liang, Y. Yan, X. Tian, X. Li, Fabrication of hybrid hydrogels from silk fibroin and tannic acid with enhanced gelation and antibacterial activities, ACS Biomater. Sci. Eng. 5 (9) (2019) 4601–4611.

[53] Y. Wang, E.J. Jeon, J. Lee, H. Hwang, S.W. Cho, H. Lee, A phenol-amine superglue inspired by insect sclerotization process, Adv. Mater. 32 (43) (2020), e2002118.

[54] C. Cui, T. Wu, X. Chen, Y. Liu, Y. Li, Z. Xu, C. Fan, W.J.A.F.M. Liu, A Janus hydrogel wet adhesive for internal tissue repair and anti-postoperative adhesion, Adv. Funct. Mater. 30 (49) (2020), 2005689.

[55] L. Han, X. Lu, K. Liu, K. Wang, L. Fang, L.T. Weng, H. Zhang, Y. Tang, F. Ren, C. Zhao, G. Sun, R. Liang, Z. Li, Mussel-inspired adhesive and tough hydrogel based on nanoclay confined dopamine polymerization, ACS Nano 11 (3) (2017) 2561–2574.

[56] L. Han, K. Liu, M. Wang, K. Wang, L. Fang, H. Chen, J. Zhou, X.J.A.F.M. Lu, Mussel-inspired adhesive and conductive hydrogel with long-lasting moisture and extreme temperature tolerance, Adv. Funct. Mater. 28 (3) (2018), 1704195.

[57] P. Zhao, K. Wei, Q. Feng, H. Chen, D.S.H. Wong, X. Chen, C.C. Wu, L. Bian, Mussel-mimetic hydrogels with defined cross-linkers achieved via controlled

catechol dimerization exhibiting tough adhesion for wet biological tissues, Chem. Commun. 53 (88) (2017) 12000–12003.
[58] B. Saleh, H.K. Dhaliwal, R. Portillo-Lara, E. Shirzaei Sani, R. Abdi, M.M. Amiji, N. Annabi, Local immunomodulation using an adhesive hydrogel loaded with miRNA-laden nanoparticles promotes wound healing, Small 15 (36) (2019), e1902232.
[59] Y. Yang, Y. Liang, J. Chen, X. Duan, B. Guo, Mussel-inspired adhesive antioxidant antibacterial hemostatic composite hydrogel wound dressing via photo-polymerization for infected skin wound healing, Bioact. Mater. 8 (2022) 341–354.
[60] X. Peng, X. Xia, X. Xu, X. Yang, B. Yang, P. Zhao, W. Yuan, P.W.Y. Chiu, L. Bian, Ultrafast self-gelling powder mediates robust wet adhesion to promote healing of gastrointestinal perforations, Sci. Adv. 7 (23) (2021), eabe8739.
[61] C.Y. Cui, T.L. Wu, X.Y. Chen, Y. Liu, Y. Li, Z.Y. Xu, C.C. Fan, W.G. Liu, A janus hydrogel wet adhesive for internal tissue repair and anti-postoperative adhesion, Adv. Funct. Mater. 30 (49) (2020), 2005689.
[62] Y.N. Jiang, X. Zhang, W. Zhang, M.H. Wang, L.W. Yan, K.F. Wang, L. Han, X. Lu, Infant skin friendly adhesive hydrogel patch activated at body temperature for bioelectronics securing and diabetic wound healing, ACS Nano 16 (6) (2022) 8662–8676.
[63] D.E. Fullenkamp, J.G. Rivera, Y.K. Gong, K.H. Lau, L. He, R. Varshney, P. B. Messersmith, Mussel-inspired silver-releasing antibacterial hydrogels, Biomaterials 33 (15) (2012) 3783–3791.
[64] A.S. Veiga, J.P. Schneider, Antimicrobial hydrogels for the treatment of infection, Biopolymers 100 (6) (2013) 637–644.
[65] Y. Bo, L. Zhang, Z. Wang, J. Shen, Z. Zhou, Y. Yang, Y. Wang, J. Qin, Y. He, Antibacterial hydrogel with self-healing property for wound-healing applications, ACS Biomater. Sci. Eng. 7 (11) (2021) 5135–5143.
[66] P. Ramburrun, N.A. Pringle, A. Dube, R.Z. Adam, S. D'Souza, M. Aucamp, Recent advances in the development of antimicrobial and antifouling biocompatible materials for dental applications, Materials 14 (12) (2021) 3167.
[67] J.L. Guo, Y. Ping, H. Ejima, K. Alt, M. Meissner, J.J. Richardson, Y. Yan, K. Peter, D. von Elverfeldt, C.E. Hagemeyer, F. Caruso, Engineering multifunctional capsules through the assembly of metal-phenolic networks, Angew. Chem., Int. Ed. 53 (22) (2014) 5546–5551.
[68] P.S. Yavvari, S. Pal, S. Kumar, A. Kar, A.K. Awasthi, A. Naaz, A. Srivastava, A. Bajaj, Injectable, self-healing chimeric catechol-Fe(III) hydrogel for localized combination cancer therapy, ACS Biomater. Sci. Eng. 3 (12) (2017) 3404–3413.
[69] C. Pucci, C. Martinelli, D. De Pasquale, M. Battaglini, N. di Leo, A. Degl'Innocenti, M. Belenli Gumus, F. Drago, G. Ciofani, Tannic acid-iron complex-based nanoparticles as a novel tool against oxidative stress, ACS Appl. Mater. Interfaces 14 (14) (2022) 15927–15941.
[70] B. Song, L. Yang, L. Han, L. Jia, Metal ion-chelated tannic acid coating for hemostatic dressing, Materials 12 (11) (2019).
[71] L. Szabó, S. Gerber-Lemaire, C. Wandrey, Strategies to functionalize the anionic biopolymer Na-alginate without restricting its polyelectrolyte properties, Polymers 12 (4) (2020) 919.
[72] H.Y. Chung, R.H. Grubbs, Rapidly cross-linkable DOPA containing terpolymer adhesives and PEG-based cross-linkers for biomedical applications, Macromolecules 45 (24) (2012) 9666–9673.
[73] J. He, Z. Zhang, Y. Yang, F. Ren, J. Li, S. Zhu, F. Ma, R. Wu, Y. Lv, G. He, B. Guo, D. Chu, Injectable self-healing adhesive pH-responsive hydrogels accelerate gastric hemostasis and wound healing, Nano-Micro Lett. 13 (1) (2021) 80.
[74] S.B. Bae, E. Kim, K. Chathuranga, J.S. Lee, W.H. Park, Gelation and the antioxidant and antibacterial properties of silk fibroin/tannic acid/Zn2+ mixtures, Polymer 230 (2021), 124090.
[75] B. Kaczmarek, Tannic acid with antiviral and antibacterial activity as A promising component of biomaterials-A minireview, Materials 13 (14) (2020).
[76] N. Ninan, A. Forget, V.P. Shastri, N.H. Voelcker, A. Blencowe, Antibacterial and anti-inflammatory pH-responsive tannic acid-carboxylated agarose composite hydrogels for wound healing, ACS Appl. Mater. Interfaces 8 (42) (2016) 28511–28521.
[77] M.V. Lomova, A.I. Brichkina, M.V. Kiryukhin, E.N. Vasina, A.M. Pavlov, D. A. Gorin, G.B. Sukhorukov, M.N. Antipina, Multilayer capsules of bovine serum albumin and tannic acid for controlled release by enzymatic degradation, ACS Appl. Mater. Interfaces 7 (22) (2015) 11732–11740.
[78] H.L. Fan, L. Wang, X.D. Feng, Y.Z. Bu, D.C. Wu, Z.X. Jin, Supramolecular hydrogel formation based on tannic acid, Macromolecules 50 (2) (2017) 666–676.
[79] L. Zhao, Z. Ren, X. Liu, Q. Ling, Z. Li, H. Gu, A multifunctional, self-healing, self-adhesive, and conductive sodium alginate/poly(vinyl alcohol) composite hydrogel as a flexible strain sensor, ACS Appl. Mater. Interfaces 13 (9) (2021) 11344–11355.
[80] X. Du, L. Wu, H. Yan, L. Qu, L. Wang, X. Wang, S. Ren, D. Kong, L. Wang, Multifunctional hydrogel patch with toughness, tissue adhesiveness, and antibacterial activity for sutureless wound closure, ACS Biomater. Sci. Eng. 5 (5) (2019) 2610–2620.
[81] B. Liu, Y. Wang, Y. Miao, X. Zhang, Z. Fan, G. Singh, X. Zhang, K. Xu, B. Li, Z. Hu, M. Xing, Hydrogen bonds autonomously powered gelatin methacrylate hydrogels with super-elasticity, self-heal and underwater self-adhesion for sutureless skin and stomach surgery and E-skin, Biomaterials 171 (2018) 83–96.
[82] F.B. Kadumudi, M. Hasany, M.K. Pierchala, M. Jahanshahi, N. Taebnia, M. Mehrali, C.F. Mitu, M.A. Shahbazi, T.G. Zsurzsan, A.J.A.M. Knott, The manufacture of unbreakable bionics via multifunctional and self-healing silk–graphene hydrogels, Adv. Mater. 33 (35) (2021), 2100047.
[83] Y.N. Chen, L. Peng, T. Liu, Y. Wang, S. Shi, H. Wang, Poly(vinyl alcohol)-tannic acid hydrogels with excellent mechanical properties and shape memory behaviors, ACS Appl. Mater. Interfaces 8 (40) (2016) 27199–27206.
[84] J.Y. Sun, X. Zhao, W.R. Illeperuma, O. Chaudhuri, K.H. Oh, D.J. Mooney, J. J. Vlassak, Z. Suo, Highly stretchable and tough hydrogels, Nature 489 (7414) (2012) 133–136.
[85] H. Fan, J. Wang, Q. Zhang, Z. Jin, Tannic acid-based multifunctional hydrogels with facile adjustable adhesion and cohesion contributed by polyphenol supramolecular chemistry, ACS Omega 2 (10) (2017) 6668–6676.
[86] L.K. Charkoudian, K.J.J.I.C. Franz, Fe (III)-coordination Properties of Neuromelanin Components: 5, 6-dihydroxyindole and 5, 6-Dihydroxyindole-2-Carboxylic Acid,, 45, 2006, pp. 3657–3664, 9.
[87] K. Kim, M. Shin, M.Y. Koh, J.H. Ryu, M.S. Lee, S. Hong, H. Lee, TAPE: a medical adhesive inspired by a ubiquitous compound in plants, Adv. Funct. Mater. 25 (16) (2015) 2402–2410.
[88] N. Holten-Andersen, M.J. Harrington, H. Birkedal, B.P. Lee, P.B. Messersmith, K. Y. Lee, J.H. Waite, pH-induced metal-ligand cross-links inspired by mussel yield self-healing polymer networks with near-covalent elastic moduli, Proc. Natl. Acad. Sci. U. S. A. 108 (7) (2011) 2651–2655.
[89] J. Guo, W. Sun, J.P. Kim, X. Lu, Q. Li, M. Lin, O. Mrowczynski, E.B. Rizk, J. Cheng, G. Qian, J. Yang, Development of tannin-inspired antimicrobial bioadhesives, Acta Biomater. 72 (2018) 35–44.
[90] Z. Jia, X. Lv, Y. Hou, K. Wang, F. Ren, D. Xu, Q. Wang, K. Fan, C. Xie, X. Lu, Mussel-inspired nanozyme catalyzed conductive and self-setting hydrogel for adhesive and antibacterial bioelectronics, Bioact. Mater. 6 (9) (2021) 2676–2687.
[91] D.A. Wang, S. Varghese, B. Sharma, I. Strehin, S. Fermanian, J. Gorham, D. H. Fairbrother, B. Cascio, J.H. Elisseeff, Multifunctional chondroitin sulphate for cartilage tissue-biomaterial integration, Nat. Mater. 6 (5) (2007) 385–392.
[92] J.M. Reyes, S. Herretes, A. Pirouzmanesh, D.A. Wang, J.H. Elisseeff, A. Jun, P. J. McDonnell, R.S. Chuck, A. Behrens, A modified chondroitin sulfate aldehyde adhesive for sealing corneal incisions, Invest. Ophthalmol. Vis. Sci. 46 (4) (2005) 1247–1250.
[93] N. Artzi, T. Shazly, A.B. Baker, A. Bon, E.R. Edelman, Aldehyde-amine chemistry enables modulated biosealants with tissue-specific adhesion, Adv. Mater. 21 (32–33) (2009) 3399–3403.
[94] Z. Zhang, X. Wang, Y. Wang, J. Hao, Rapid-forming and self-healing agarose-based hydrogels for tissue adhesives and potential wound dressings, Biomacromolecules 19 (3) (2018) 980–988.
[95] M.A. Spring, Use of a lysine-derived urethane surgical adhesive as an alternative to progressive tension sutures in abdominoplasty patients: a cohort study, Aesthetic Surg. J. 38 (12) (2018) 1318–1329.
[96] A.I. Bochyńska, S. Sharifi, T.G. van Tienen, P. Buma, D.W. Grijpma, Development of tissue adhesives based on amphiphilic isocyanate-terminated trimethylene carbonate block copolymers, Macromol. Symp. 334 (1) (2013) 40–48.
[97] K. Ono, Y. Saito, H. Yura, K. Ishikawa, A. Kurita, T. Akaike, M. Ishihara, Photocrosslinkable chitosan as a biological adhesive, J. Biomed. Mater. Res. 49 (2) (2000) 289–295.
[98] B.P. Lee, P.B. Messersmith, J.N. Israelachvili, J.H. Waite, Mussel-inspired adhesives and coatings, Annu. Rev. Mater. Res. 41 (2011) 99–132.
[99] E.W. Danner, Y. Kan, M.U. Hammer, J.N. Israelachvili, J.H. Waite, Adhesion of mussel foot protein Mefp-5 to mica: an underwater superglue, Biochemistry 51 (33) (2012) 6511–6518.
[100] A.R. Narkar, J.D. Kelley, R. Pinnaratip, B.P. Lee, Effect of ionic functional groups on the oxidation state and interfacial binding property of catechol-based adhesive, Biomacromolecules 19 (5) (2018) 1416–1424.
[101] Y.J. Xu, K.C. Wei, P.C. Zhao, Q. Feng, C.K.K. Choi, L.M. Bian, Preserving the adhesion of catechol-conjugated hydrogels by thiourea-quinone coupling, Biomater. Sci. 4 (12) (2016) 1726–1730.
[102] T.H. Anderson, J. Yu, A. Estrada, M.U. Hammer, J.H. Waite, J.N. Israelachvili, The contribution of DOPA to substrate-peptide adhesion and internal cohesion of mussel-inspired synthetic peptide films, Adv. Funct. Mater. 20 (23) (2010) 4196–4205.
[103] T. Priemel, R. Palia, M. Babych, C.J. Thibodeaux, S. Bourgault, M.J. Harrington, Compartmentalized processing of catechols during mussel byssus fabrication determines the destiny of DOPA, Proc. Natl. Acad. Sci. U. S. A. 117 (14) (2020) 7613–7621.
[104] A. Cholewinski, F. Yang, B.X. Zhao, Algae-mussel-inspired hydrogel composite glue for underwater bonding, Mater. Horiz. 6 (2) (2019) 285–293.
[105] D.S. Hwang, H. Zeng, A. Masic, M.J. Harrington, J.N. Israelachvili, J.H. Waite, Protein- and metal-dependent interactions of a prominent protein in mussel adhesive plaques, J. Biol. Chem. 285 (33) (2010) 25850–25858.
[106] J. Yu, W. Wei, E. Danner, R.K. Ashley, J.N. Israelachvili, J.H. Waite, Mussel protein adhesion depends on interprotein thiol-mediated redox modulation, Nat. Chem. Biol. 7 (9) (2011) 588–590.
[107] B. Yang, C. Lim, D.S. Hwang, H.J. Cha, Switch of surface adhesion to cohesion by dopa-Fe3+ complexation, in response to microenvironment at the mussel plaque/substrate interface, Chem. Mater. 28 (21) (2016) 7982–7989.
[108] J.J. Moon, M.S. Hahn, I. Kim, B.A. Nsiah, J.L. West, Micropatterning of poly (ethylene glycol) diacrylate hydrogels with biomolecules to regulate and guide endothelial morphogenesis, Tissue engineering, Part A 15 (3) (2009) 579–585.
[109] K.S. Liu, Preparation of fatty-acid methyl esters for gas-chromatographic analysis of lipids in biological-materials, J. Am. Oil Chem. Soc. 71 (11) (1994) 1179–1187.
[110] D.D. Ramey, C.S. Ough, Volatile ester hydrolysis or formation during storage of model solutions and wines, J. Agric. Food Chem. 28 (5) (1980) 928–934.

[111] H. Jafari, P. Ghaffari-Bohlouli, D. Podstawczyk, L. Nie, A. Shavandi, Tannic acid post-treatment of enzymatically crosslinked chitosan-alginate hydrogels for biomedical applications, Carbohydr. Polym. 295 (2022), 119844.
[112] L. Zhang, Y. Zhang, F. Ma, X. Liu, Y. Liu, Y. Cao, R. Pei, A low-swelling and toughened adhesive hydrogel with anti-microbial and hemostatic capacities for wound healing, J. Mater. Chem. B 10 (6) (2022) 915–926.
[113] Q. Zeng, F. Wang, R. Hu, X. Ding, Y. Lu, G. Shi, H. Haick, M. Zhang, Debonding-on-demand polymeric wound patches for minimal adhesion and clinical communication, Adv. Sci. 9 (29) (2022), e2202635.
[114] Y. Zhang, T.H. Tao, Skin-Friendly Electronics for Acquiring Human Physiological Signatures 31 (49) (2019), 1905767.
[115] Y. Zhou, M. Chen, Q. Ban, Z. Zhang, S. Shuang, K. Koynov, H.-J.r. Butt, J. Kong, S. J.A.M.L. Wu, Light-switchable Polymer Adhesive Based on Photoinduced Reversible Solid-To-Liquid Transitions, 8, 2019, pp. 968–972, 8.
[116] J. Huang, Y. Liu, Y. Yang, Z. Zhou, J. Mao, T. Wu, J. Liu, Q. Cai, C. Peng, Y.J.S. R. Xu, Electrically programmable adhesive hydrogels for climbing robots 6 (53) (2021), eabe1858.
[117] T. Xie, J. Ding, X.X. Han, H.Z. Jia, Y. Yang, S. Liang, W.X. Wang, W.G. Liu, W. Wang, Wound dressing change facilitated by spraying zinc ions, Mater. Horiz. 7 (2) (2020) 605–614.
[118] Y. Zhao, Y. Wu, L. Wang, M. Zhang, X. Chen, M. Liu, J. Fan, J. Liu, F. Zhou, Z. Wang, Bio-inspired reversible underwater adhesive, Nat. Commun. 8 (1) (2017) 2218.
[119] P.E. Hallaway, J.W. Eaton, S.S. Panter, B.E. Hedlund, Modulation of deferoxamine toxicity and clearance by covalent attachment to biocompatible polymers, Proc. Natl. Acad. Sci. U. S. A. 86 (24) (1989) 10108–10112.
[120] D.E. Atkinson, M.N. Camien, The role or urea synthesis in the removal of metabolic bicarbonate and the regulation of blood pH, Curr. Top. Cell. Regul. 21 (1982) 261–302.
[121] B. Yang, L. Bankir, Urea and urine concentrating ability: new insights from studies in mice, Am. J. Physiol. Ren. Physiol. 288 (5) (2005) F881–F896.
[122] F.A. Andersen, Final report of the safety assessment of urea, Int. J. Toxicol. 24 (3) (2005) 1–56.
[123] L. Celleno, Topical urea in skincare: a review, Dermatol. Ther. 31 (6) (2018), e12690.
[124] F. Viola, G. Barteselli, L. Dell'arti, D. Vezzola, E. Villani, C. Mapelli, L. Zanaboni, M.D. Cappellini, R. Ratiglia, Abnormal fundus autofluorescence results of patients in long-term treatment with deferoxamine, Ophthalmology 119 (8) (2012) 1693–1700.
[125] M. Selim, L.D. Foster, C.S. Moy, G. Xi, M.D. Hill, L.B. Morgenstern, S. M. Greenberg, M.L. James, V. Singh, W.M. Clark, C. Norton, Y.Y. Palesch, S. D. Yeatts, D.E.F.I. i, Deferoxamine mesylate in patients with intracerebral haemorrhage (i-DEF): a multicentre, randomised, placebo-controlled, double-blind phase 2 trial, Lancet Neurol. 18 (5) (2019) 428–438.
[126] P.N. Dilly, Structure and function of the tear film, Adv. Exp. Med. Biol. 350 (1994) 239–247.
[127] M. Gulino, D. Kim, S. Pane, S.D. Santos, A.P. Pego, Tissue response to neural implants: the use of model systems toward new design solutions of implantable microelectrodes, Front. Neurosci. 13 (2019) 689.
[128] P. Rejmontova, Z. Capakova, N. Mikusova, N. Marakova, V. Kasparkova, M. Lehocky, P. Humpolicek, Adhesion, proliferation and migration of NIH/3T3 cells on modified polyaniline surfaces, Int. J. Mol. Sci. 17 (9) (2016) 1439.
[129] G. Ciapetti, E. Cenni, D. Cavedagna, L. Pratelli, A. Pizzoferrato, Cell-culture methods to evaluate the biocompatibility of implant materials, ATLA, Altern. Lab. Anim. 20 (1) (1992) 52–60.
[130] E. Rosellini, N. Barbani, L. Lazzeri, M.G. Cascone, Biomimetic and bioactive small diameter tubular scaffolds for vascular tissue engineering, Biomimetics 7 (4) (2022) 199.
[131] Y.Z. Fang, S. Yang, G. Wu, Free radicals, antioxidants, and nutrition, Nutrition 18 (10) (2002) 872–879.
[132] M.M. Chang, X.X. Liu, X.H. Wang, F. Peng, J.L. Ren, Mussel-inspired adhesive hydrogels based on biomass-derived xylan and tannic acid cross-linked with acrylic acid with antioxidant and antibacterial properties, J. Mater. Sci. 56 (26) (2021) 14729–14740.
[133] R.G. Andrade Jr., L.T. Dalvi, J.M. Silva Jr., G.K. Lopes, A. Alonso, M. Hermes-Lima, The antioxidant effect of tannic acid on the in vitro copper-mediated formation of free radicals, Arch. Biochem. Biophys. 437 (1) (2005) 1–9.
[134] C.Y. Mao, Y.M. Xiang, X.M. Liu, Z.D. Cui, X.J. Yang, K.W.K. Yeung, H.B. Pan, X. B. Wang, P.K. Chu, S.L. Wu, Photo-inspired antibacterial activity and wound healing acceleration by hydrogel embedded with Ag/Ag@AgCl/ZnO nanostructures, ACS Nano 11 (9) (2017) 9010–9021.
[135] X.J. Zhu, W. Feng, J. Chang, Y.W. Tan, J.C. Li, M. Chen, Y. Sun, F.Y. Li, Temperature-feedback upconversion nanocomposite for accurate photothermal therapy at facile temperature, Nat. Commun. 7 (1) (2016) 1–10.
[136] H.M. Yehia, E.A. Ismail, Z.K. Hassan, A.H. Al-Masoud, M.M. Al-Dagal, Heat resistance and presence of genes encoding staphylococcal enterotoxins evaluated by multiplex-PCR of Staphylococcus aureus isolated from pasteurized camel milk, Biosci. Rep. 39 (11) (2019).
[137] S. Chen, C. Xing, D. Huang, C. Zhou, B. Ding, Z. Guo, Z. Peng, D. Wang, X. Zhu, S. J.S.a. Liu, Eradication of tumor growth by delivering novel photothermal selenium-coated tellurium, nanoheterojunctions 6 (15) (2020), eaay6825.
[138] Y. Yang, W. Zhu, Z. Dong, Y. Chao, L. Xu, M. Chen, Z. Liu, 1D coordination polymer nanofibers for low-temperature photothermal therapy, Adv. Mater. 29 (40) (2017), 1703588.
[139] S.K. Calderwood, Hyperthermia, the Tumor Microenvironment and Immunity, Tumor Ablation, Springer, 2013, pp. 29–37.
[140] Y. Zhao, X.M. Dai, X.S. Wei, Y.J. Yu, X.L. Chen, X.E. Zhang, C.X. Li, Near-infrared light-activated thermosensitive liposomes as efficient agents for photothermal and antibiotic synergistic therapy of bacterial biofilm, ACS Appl. Mater. Interfaces 10 (17) (2018) 14426–14437.
[141] G. Feller, E. Narinx, J.L. Arpigny, Z. Zekhnini, J. Swings, C. Gerday, Temperature-dependence of growth, enzyme-secretion and activity of psychrophilic antarctic bacteria, Appl. Microbiol. Biotechnol. 41 (4) (1994) 477–479.
[142] X.J. Zhu, W. Feng, J. Chang, Y.W. Tan, J.C. Li, M. Chen, Y. Sun, F.Y. Li, Temperature-feedback upconversion nanocomposite for accurate photothermal therapy at facile temperature, Nat. Commun. 7 (1) (2016) 1–10.
[143] G. Gao, Y.W. Jiang, H.R. Jia, F.G. Wu, Near-infrared light-controllable on-demand antibiotics release using thermo-sensitive hydrogel-based drug reservoir for combating bacterial infection, Biomaterials 188 (2019) 83–95.
[144] H. Lee, S. Chung, M.G. Kim, L.P. Lee, J.Y. Lee, Near-infrared-light-assisted photothermal polymerization for transdermal hydrogelation and cell delivery, Adv Healthc Mater 5 (13) (2016) 1638–1645.
[145] J. Fang, Y. Wan, Y. Sun, X.L. Sun, M.L. Qi, S. Cheng, C.Y. Li, Y.M. Zhou, L. Xu, B. Dong, L. Wang, Near-infrared-activated nanohybrid coating with black phosphorus/zinc oxide for efficient biofilm eradication against implant-associated infections, Chem. Eng. J. 435 (2022), 134935.
[146] M.X. Ma, X.M. Liu, L. Tan, Z.D. Cui, X.J. Yang, Y.Q. Liang, Z.Y. Li, Y.F. Zheng, K. W.K. Yeung, S.L. Wu, Enhancing the antibacterial efficacy of low-dose gentamicin with 5 minute assistance of photothermy at 50 degrees C, Biomater. Sci. 7 (4) (2019) 1437–1447.
[147] Y. Yang, X. Zhou, Y.K. Chan, Z. Wang, L. Li, J. Li, K. Liang, Y. Deng, Photo-Activated nanofibrous membrane with self-rechargeable antibacterial function for stubborn infected cutaneous regeneration, Small 18 (12) (2022), e2105988.
[148] G. Zhang, X. Zhang, Y. Yang, R. Chi, J. Shi, R. Hang, X. Huang, X. Yao, P.K. Chu, X. Zhang, Dual light-induced in situ antibacterial activities of biocompatibleTiO (2)/MoS(2)/PDA/RGD nanorod arrays on titanium, Biomater. Sci. 8 (1) (2020) 391–404.
[149] P. Li, W. She, Y. Luo, D. He, J. Chen, N. Ning, Y. Yu, S. de Beer, S. Zhang, One-pot, self-catalyzed synthesis of self-adherent hydrogels for photo-thermal, antimicrobial wound treatment, J. Mater. Chem. B 9 (1) (2021) 159–169.
[150] X. Zhao, Y.P. Liang, Y. Huang, J.H. He, Y. Han, B.L. Guo, Physical double-network hydrogel adhesives with rapid shape adaptability, fast self-healing, antioxidant and NIR/pH stimulus-responsiveness for multidrug-resistant bacterial infection and removable wound dressing, Adv. Funct. Mater. 30 (17) (2020), 1910748.
[151] N. Yang, M. Zhu, G. Xu, N. Liu, C. Yu, A near-infrared light-responsive multifunctional nanocomposite hydrogel for efficient and synergistic antibacterial wound therapy and healing promotion, J. Mater. Chem. B 8 (17) (2020) 3908–3917.
[152] C. Tong, X. Zhong, Y. Yang, X. Liu, G. Zhong, C. Xiao, B. Liu, W. Wang, X. Yang, PB@PDA@Ag nanosystem for synergistically eradicating MRSA and accelerating diabetic wound healing assisted with laser irradiation, Biomaterials 243 (2020), 119936.
[153] Z. Li, S. You, R. Mao, Y. Xiang, E. Cai, H. Deng, J. Shen, X. Qi, Architecting polyelectrolyte hydrogels with Cu-assisted polydopamine nanoparticles for photothermal antibacterial therapy, Mater Today Bio 15 (2022), 100264.
[154] C.B. Wang, Y.Q. Liang, Y. Huang, M. Li, B.L. Guo, Porous photothermal antibacterial antioxidant dual - crosslinked cryogel based on hyaluronic acid/polydopamine for non-compressible hemostasis and infectious wound repair, J. Mater. Sci. Technol. 121 (2022) 207–219.
[155] X. Xu, X. Liu, L. Tan, Z. Cui, X. Yang, S. Zhu, Z. Li, X. Yuan, Y. Zheng, K.W. K. Yeung, P.K. Chu, S. Wu, Controlled-temperature photothermal and oxidative bacteria killing and acceleration of wound healing by polydopamine-assisted Au-hydroxyapatite nanorods, Acta Biomater. 77 (2018) 352–364.
[156] Y. Huang, L. Mu, X. Zhao, Y. Han, B. Guo, Bacterial growth-induced tobramycin smart release self-healing hydrogel for Pseudomonas aeruginosa-infected burn wound healing, ACS Nano 16 (8) (2022) 13022–13036.
[157] Y. Ye, J. He, Y. Qiao, Y. Qi, H. Zhang, H.A. Santos, D. Zhong, W. Li, S. Hua, W. Wang, A. Grzybowski, K. Yao, M. Zhou, Mild temperature photothermal assisted anti-bacterial and anti-inflammatory nanosystem for synergistic treatment of post-cataract surgery endophthalmitis, Theranostics 10 (19) (2020) 8541–8557.
[158] M. Li, Y.P. Liang, J.H. He, H.L. Zhang, B.L. Guo, Two-pronged strategy of biomechanically active and biochemically multifunctional hydrogel wound dressing to accelerate wound closure and wound healing, Chem. Mater. 32 (23) (2020) 9937–9953.